Expanding influence of Atlantic and Pacific ocean heat transport on Arctic winter sea ice variability

Jakob Dörr [1,3], Marius Årthun [1,3], Tor Eldevik [1,3], Anne Britt Sandø [2,3]

[1]Geophysical Institute, University of Bergen, Norway
[2]Institute for Marine Research, Bergen, Norway
[3]Bjerknes Centre for Climate Research, Bergen, Norway

Key Points:

- The influence of Barents Sea Opening and Bering Strait ocean heat transport on winter sea ice variability will expand in the future
- The Lomonosov Ridge separates the future influence regions of Pacific and Atlantic waters
- Differences in the projected future influence are related to inflow properties, sea ice loss, and upper ocean stratification

Corresponding author: Jakob Dörr, jakob.dorr@uib.no

Abstract

The general retreat of Arctic sea ice is overlaid by large year-to-year variability. In winter, sea ice loss and variability are currently most pronounced in the Barents Sea, primarily due to variable ocean heat transport from the Atlantic. As the loss of winter Arctic sea ice is expected to continue and the sea ice edge retreats deeper into the Arctic Ocean, other regions will experience increased sea-ice variability until essentially ice-free. However, it remains to be established to what extent future winter sea ice loss beyond the Barents Sea is facilitated by ocean heat transport. To answer this question, we analyze and contrast the present and future regional impact of Pacific and Atlantic ocean heat transport on the winter Arctic sea ice cover using simulations from seven single-model large ensembles. We find strong model agreement for an expanding influence of ocean heat transport through the Bering Strait and the Barents Sea under continued sea ice retreat. Model differences can be related to mean volume transport and inflow temperature, mean sea ice state, and upper ocean stratification. Our work highlights the increasing importance of the Pacific and Atlantic water inflows to the Arctic Ocean and indicates that their future influence regions will be separated by the Lomonosov Ridge.

Plain Language Summary

The winter sea ice cover in the Arctic is slowly decreasing, but it shows a lot of variability from year to year. Some of this variability is determined by how much heat is transported into the Arctic Ocean via the Fram Strait, Barents Sea, and Bering Strait. We try to understand how the influence of this oceanic heat transport will change in the future when the sea ice retreats further into the Arctic Ocean. We compare several climate models and find that most of them show a northward expanding influence of heat transport through the Barents Sea and the Bering Strait. How much these transports still influence the future sea ice depends on how much sea ice is lost, changes in the inflowing waters, and the vertical stability of the upper layer in the Arctic Ocean.

1 Introduction

The recent retreat of the Arctic sea ice cover is overlaid by strong internal variability, particularly during the winter months (England et al., 2019; Årthun et al., 2019). This variability impacts our estimates of the forced response of sea ice to global warming and is a large source of uncertainty for projections of the sea ice cover. In winter,

a large part of the variability is driven by variable transport of oceanic heat into the Arctic Ocean (Carmack et al., 2015; Polyakov et al., 2020; Docquier & Königk, 2021). There are three main gateways. Water from the Nordic Seas - and Atlantic ocean upstream - flows into the Arctic Ocean either through the Fram Strait or the Barents Sea Opening (BSO, Fig. 1). On the other side of the Arctic, Pacific water enters the shallow Chukchi shelf through the 50 m deep Bering Strait (Fig. 1). While the water flowing into the Fram Strait typically subducts under the halocline north of Svalbard (Rudels et al., 2015) and has limited influence on winter sea ice (Lundesgaard et al., 2021; Dörr et al., 2021), water flowing through the BSO enters the shallow Barents Sea shelf where it may occupy the entire water column and affect the winter sea ice in the Barents Sea and beyond (Schlichtholz, 2011; Årthun et al., 2019). Oceanic heat transported through the Bering Strait has the potential to melt large quantities of sea ice (Woodgate, 2018; Serreze et al., 2019; Y. Wang et al., 2021) and impacts the early winter sea ice advance in the Chukchi Sea (Serreze et al., 2016).

Over the next decades, the Arctic will likely become ice-free in summer (Community, 2020) and the sea ice in winter will retreat further into the interior Arctic Ocean, although there is substantial uncertainty about the timing and extent of the winter sea ice loss (Årthun et al., 2021). As a consequence, the interior Arctic Ocean will be more directly affected by changes in the Pacific and Atlantic Water inflows, an effect named borealization (Polyakov et al., 2020), or – split up into the two regional influences – atlantification and pacification (Årthun et al., 2012; Polyakov et al., 2017; Dörr et al., 2021). It is therefore important to understand the changing influence of ocean heat transport on sea ice, not only because it will potentially affect our ability to predict sea ice changes, but also because it is a key driver and indicator of ongoing borealization.

Using the Community Earth System Model Large Ensemble (CESM-LE), Dörr et al. (2021) documented the possible future atlantification and pacification through a projected expanding influence of ocean heat transport on winter sea ice under a high emissions scenario. The changes in CESM-LE are carried by an expanding influence of ocean heat transport through the Barents Sea on the Atlantic side and through the Bering Strait on the Pacific side, while the influence of Fram Strait heat transport stays weak. However, the inference was only based on a single model ensemble, a broader comparison of these future changes for several models has not been performed, and possible sources of model differences have not been assessed. Here, we, therefore, compare changes in 7 sin-

gle model ensembles from both the fifth (CMIP5) and the sixth (CMIP6) phase of the Coupled Model Intercomparison Project.

It also remains unresolved to what extent future borealization is a manifestation of a stronger and warmer Atlantic inflow (Årthun et al., 2019; Dörr et al., 2021) or enhanced upward fluxes of ocean heat as a result of weakened stratification (Polyakov et al., 2017; Lind et al., 2018). A sustained and possibly increased incursion of Atlantic waters into the Eurasian Basin throughout the century is expected (Shu et al., 2021), which could act to weaken upper-ocean stratification and increase vertical heat fluxes, and, hence, lead to a thinner and less extensive sea-ice cover. However, the sea ice is generally shielded from warm Atlantic water below by a cold layer that is strongly stratified in salinity, i.e., the cold halocline (Rudels et al., 2015). Variability in the properties of this insulating layer can therefore vary the effect of warm Atlantic and Pacific waters on regional sea ice evolution. Furthermore, the surface ocean in parts of the Arctic Ocean is expected to become fresher in the future due to increased freshwater fluxes, precipitation, and river runoff (Rawlins et al., 2010), which will act to stabilize the upper ocean, and, hence, limit the influence of Atlantic and Pacific waters. Here, we accordingly assess how inter-model differences in the strength and properties of the Atlantic and Pacific water inflows, and in the representation of upper ocean stratification are reflected in how ocean heat transport impacts future sea ice variability. This allows us to constrain the projected changes in oceanic influence and to better understand the drivers of future borealization of the Arctic Ocean.

The analysis is structured as follows: Following an overview of the methods and model data, we compare future changes in winter sea ice cover and inflow properties at the gateways in sections 3 and 4, respectively. We then compare changes in the regional influence of heat transport and set model differences in relation to mean quantities in sections 5 and 6. The discussion and summary in section 7 conclude the study.

2 Materials and Methods

We analyze and compare monthly mean model output from seven single-model large ensembles: the CESM-LE (40 members) and GFDL-CM3-LENS (20 members) based on the CMIP5 models CESM1 and GFDL-CM3, and five ensembles based on the models MPI-ESM1-2-LR (10 members), MIROC6 (20 members), ACCESS-ESM1-5 (10 mem-

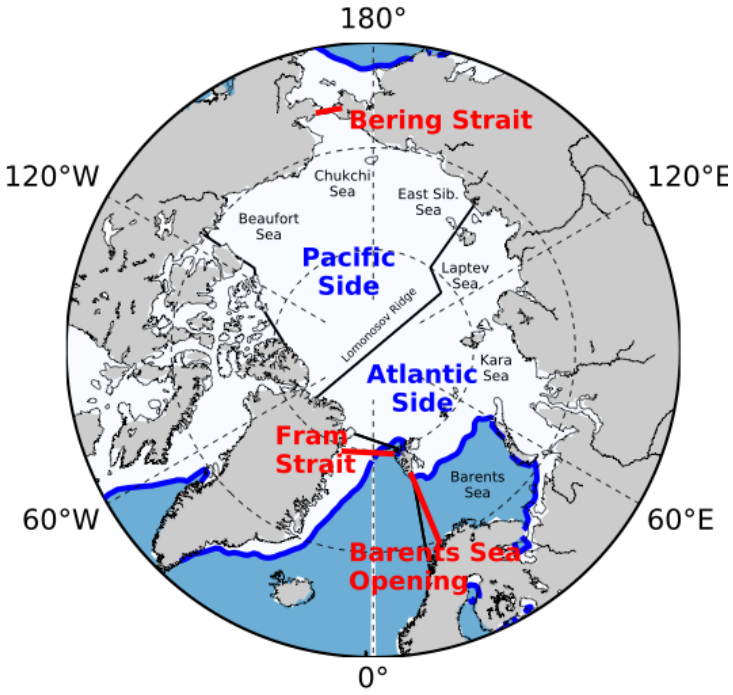

Figure 1. Map of the Arctic Ocean. White shading and the blue line represent the mean observed winter (solid) sea ice edge (based on a 50% sea ice concentration) between 1990 and 2019. Red lines indicate the three major gateways into the Arctic Ocean, and the solid black lines mark the division between the Atlantic Side and Pacific Side, which approximates the location of the Lomonosov Ridge.

Table 1. Overview of single-model ensembles used in this study.

Model	Ensemble members	High scenario	Low scenario	Reference	horizontal ocean res. north of 66°N
CESM-LE	40 high	RCP8.5	2°C	Kay et al. (2015)	45 km
	10 low			Sanderson et al. (2017)	45 km
GFDL-CM3-LENS	20	RCP8.5	–	Sun et al. (2018)	55 km
MPI-ESM1-2-LR	10	SSP5-8.5	SSP1-2.6	Mauritsen et al. (2019)	55 km
MIROC6	20	SSP5-8.5	SSP1-2.6	Tatebe et al. (2019)	40 km
ACCESS-ESM1-5	10	SSP5-8.5	SSP1-2.6	Ziehn et al. (2020)	35 km
CanESM5	10	SSP5-8.5	SSP1-2.6	Swart et al. (2019)	50 km
EC-Earth3	15	SSP5-8.5	SSP1-2.6	Döscher et al. (2021)	50 km

bers), CanESM5 (10 members) and EC-Earth3 (15 members) from CMIP6 (Eyring et al., 2016). Output from GFDL-CM3-LENS and CESM-LE is available through the Multi-Model Large Ensemble Archive (Deser et al., 2020). Additional information about the ensemble size and future scenarios is given in table 1. The CMIP6 models were chosen based on a minimum member size of 10 of available output for all the relevant variables. A sufficient ensemble size is required to robustly separate internal variability from the forced signal (Milinski et al., 2020) and a threshold of 10 members represents a trade-off between robustness and the number of available models. We analyze the historical simulations and two future scenarios: a high-emissions, high warming scenario (RCP8.5 or SSP5-8.5) for all models and additionally a low warming scenario (SSP1-2.6, also referenced to as the 2°C scenario for CESM-LE) for all models except the GFDL-CM3, where no data is available.

The ocean heat transport (OHT) through a section is defined as

$$OHT = \rho c_p \int_S \mathbf{U}(T - T_{ref}) dS, \tag{1}$$

where $\rho = 1025$ kg m^{-3} and $c_p = 4000$ J K^{-1} kg^{-1} are the constant density and heat capacity of seawater, $\mathbf{U}$ is the velocity normal to the section, T is the temperature and S the surface area of the section. We calculate the heat transport on the models' native grid using the model variables *uo*, *vo*, and *thetao*, except for CESM-LENS, where we use the advective heat flux (UET and VNT). We use a reference temperature T_{ref} of 0 °C. We calculate annual mean OHT through the Barents Sea Opening (BSO), Bering Strait, and the Fram Strait (Fig. 1).

We use observations of sea ice concentration from HadISST2 (Titchner & Rayner, 2014) from 1990–2019. Due to the shortness of the observational records of OHT, we use estimates of OHT, temperature, and salinity from the ocean reanalysis ORAS5 (Zuo et al., 2019) from 1990–2019. ORAS5 upper Arctic ocean temperatures generally agree with observations and have previously been used to study Arctic Ocean temperatures (Shu et al., 2021; Li et al., 2022). We compared OHT in ORAS5 with observed estimates based on mooring data in the Bering Strait (1999–2015, Woodgate (2018)) the BSO (1998–2016, Skagseth et al. (2020) and the Fram Strait (1998–2011, Beszczynska-Möller et al. (2012)). ORAS5 simulates a mean OHT similar to observations in all three gateways (not shown).

We analyze monthly sea ice concentration (model variables *sic*/*siconc*) and calculate the sea ice area on the Pacific (Chukchi, East Siberian and the Beaufort Sea, Central Arctic between 130°E and 50°W) and Atlantic side (Barents, Kara, and Laptev Sea, Central Arctic between 50°W and 130°E, Fig. 1) on the native model grids by summing up the product of the grid cell area and the sea ice concentration of all grid cells in the two regions. We compare the simulated sea ice concentration with estimates based on satellite observations for the period 1990–2019 from HadISST2 (Titchner & Rayner, 2014).

We isolate internal variability from the forced signal in the model ensembles by averaging over the ensemble dimension and removing the resulting ensemble mean from the raw data of each member. To compare the connection between OHT and winter sea ice, we follow Dörr et al. (2021) and correlate the annual mean OHT with sea ice concentration averaged over the following winter (November–March) for all model ensembles. We compare two time periods: A recent past (1990–2019) and a future period (2050-2079) for both high and low warming scenarios. For each time period, we concatenate the 30-year time series from each member (ensemble mean removed) and perform the correlations on the concatenated time series. Note that all correlations are reversed so

that positive correlations mean sea ice loss for an increased OHT. For the analysis of transient changes in the OHT's influence, we perform the correlations for running periods from 1990–2019 to 2050–2079 in one-year increments.

3 Present and future winter sea ice

Figure 2 shows the ensemble mean winter sea ice cover for the analyzed models. In the recent past, the models generally simulate a mean sea ice cover similar to satellite observations. On the Atlantic side, EC-Earth3 and CESM-LE simulate more ice than observed, while on the Pacific side, the GFDL-CM3 and the MIROC6 simulate less ice than observed. The MPI-ESM1-2-LR, ACCESS-ESM1-5, and the CanESM5 are broadly consistent with observations on either side, although CanESM5 has too much sea ice in the Labrador Sea.

Forced changes in the different models are represented by comparing the ensemble means from 2050–2079 with those from 1990–2019. For a high emissions scenario (SSP5-8.5 or RCP8.5), most models project a retreat of the winter mean ice edge towards the western Laptev Sea on the Atlantic side and towards the northern Chukchi Sea on the Pacific side (southern Chukchi for the MPI-ESM1-2-LR), consistent with a delayed freeze-up of the Arctic Ocean in early winter (Årthun et al., 2021). However, the CanESM5 and the GFDL-CM3 project a strong decrease in sea-ice concentration over the entire Arctic Ocean, leading to ice-free conditions during most of the winter.

Under a low emissions scenario (SSP1-2.6 and 2°C), the forced changes are smaller than for the high emissions scenarios (Fig. S1 in the online supplemental material). Most models project a retreat of the mean ice edge towards the northern Barents Sea on the Atlantic and the southern Chukchi or the northern Bering Sea on the Pacific side. CanESM5 projects a much stronger sea ice retreat than the other models on the Atlantic side.

4 Present and future ocean heat transport

The simulated evolution of ocean heat and volume transport through, and ocean temperature at, the three main Arctic gateways is shown for all models in Fig. 3. For the Barents Sea Opening, most models simulate a mean heat transport of 40–90 TW from 1990–2019, consistent with the estimate from ORAS5 of 70 TW. The forced trend is pos-

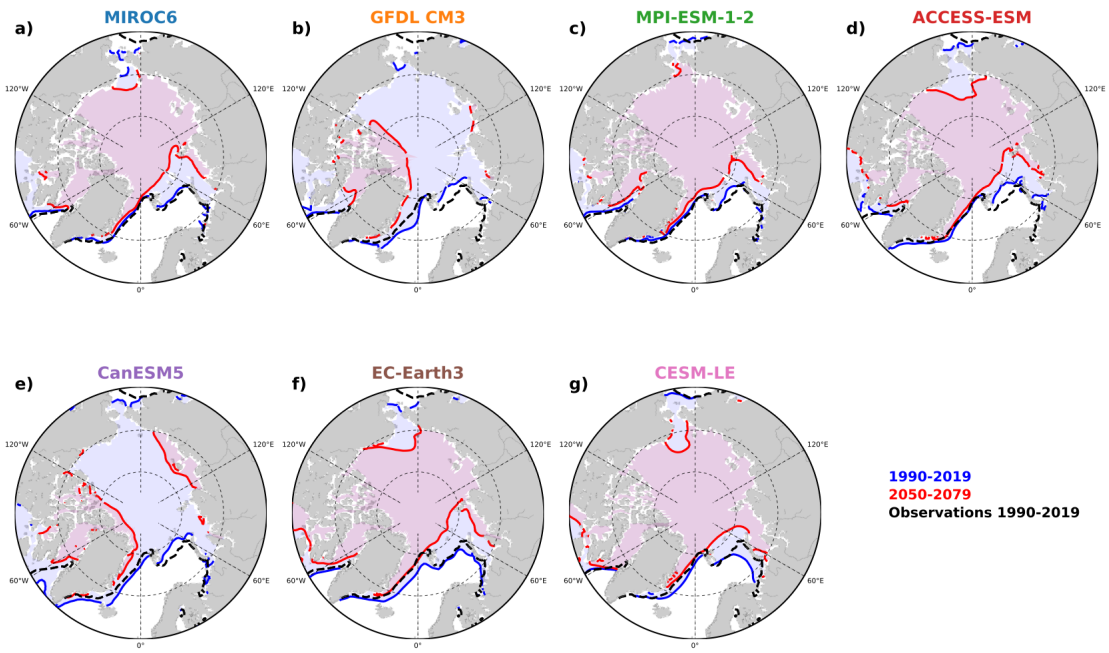

Figure 2. Present and future winter sea ice cover. Ensemble mean winter (November – March) sea ice edge (50% threshold) for 1990–2019 (blue line) and 2050–2079 (red line) for the high emissions scenario for all models. The Black dashed line shows the observed sea ice edge from 1990-2019.

itive for all models, but the EC-Earth3 and CanESM5 have by far the strongest trends. For future periods, the heat transport increases further in all models.

The OHT through the Fram Strait displays large differences among the models, values ranging from 1 TW to around 80 TW over the recent past, compared to the ORAS5 estimate of around 25 TW (Fig. 3b). All models except the MPI-ESM1-2-LR show an increase in OHT during recent decades. Most models show a forced increase in the future under the high emissions scenario, except for GFDL-CM3 which shows a decrease.

The Bering Strait OHT ranges from 1 TW to 12 TW in the models, spanning the ORAS5 estimate of 6 TW (Fig. 3c). All models simulate a positive forced trend in OHT over the recent past as well as for the future periods under the high emissions scenario. For all three gates, the projected future OHT changes are similar but slightly smaller in the low emissions scenario compared to the high emissions scenario (Fig. S2 in the online supplemental material).

Changes in OHT can be driven by changes in volume transport or changes in the inflow temperature, both of which are shown in Figure 3g-i. Models are broadly in agreement with observed volume transport and temperature in the BSO and to a lesser degree in the Bering Strait. In Fram Strait, the models simulate a weaker volume transport and a higher water temperature. In general, the forced increase in OHT is primarily driven by an increase in the water temperature in all models (Fig. 3g-i), especially for the Bering Strait, where the volume transport decreases over time in all models (Fig. 3f). For the BSO and the Fram Strait, some models also project strong increases in volume transport, which drive increased OHT. All cases of a forced decrease in OHT, which are most common for the Fram Strait, are driven by decreases in volume transport.

5 Connection between ocean heat transport and winter sea ice

To assess the future expansion of atlantification and pacification, we compare the connection between OHT and the winter sea ice cover in the model ensembles. Figure 4 shows anomaly correlations of the annual mean OHT with the following winter mean sea ice concentration for the high emissions scenario. To focus on the regions substantially influenced by ocean heat transport, we only show contours of one correlation level (r=0.4). For the recent past (1990–2019) all models show significant connections between the Bering Strait OHT and winter sea ice in the southern Chukchi Sea, and between the

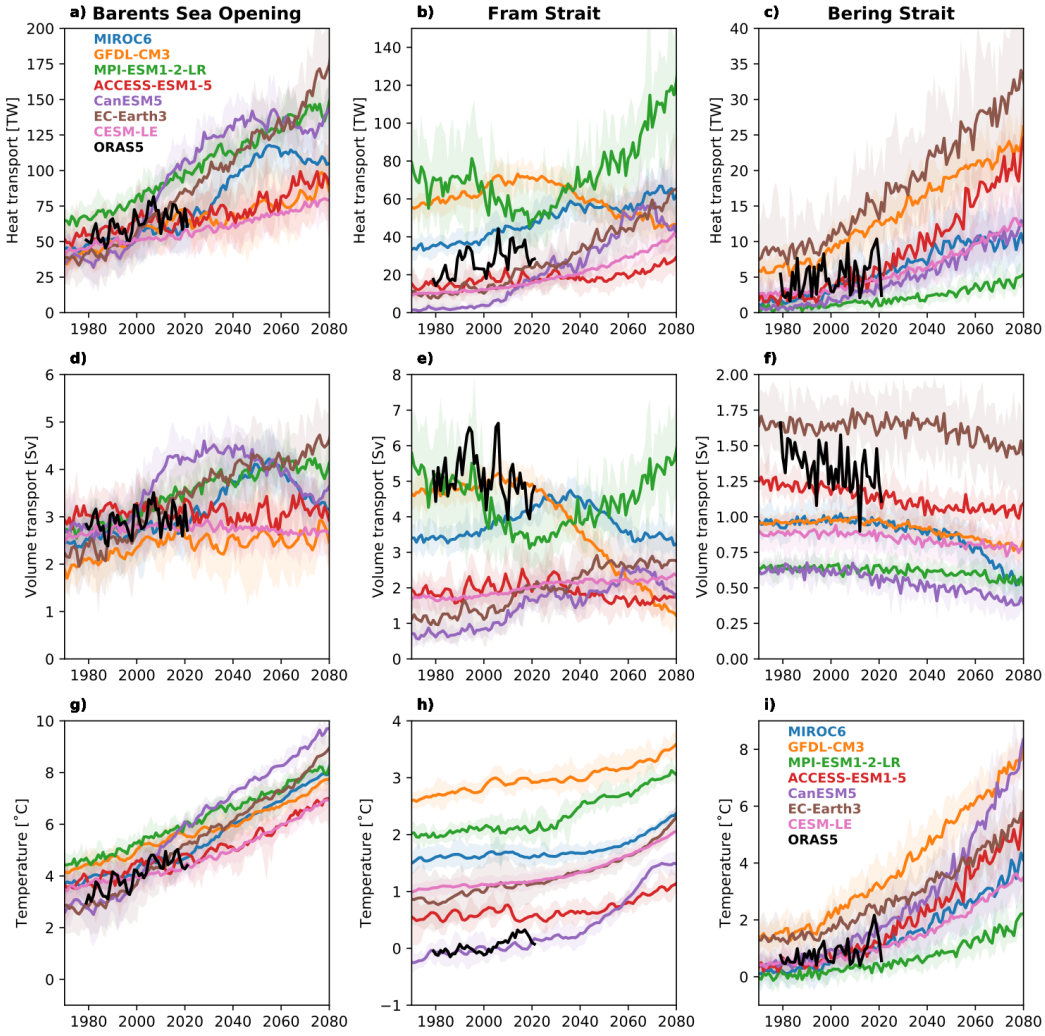

Figure 3. Present and future changes at the inflow gateways. Time series of annual mean a-c) heat transport, d-f) volume transport and g-i) water temperature at the three gateways for ORAS5 (black line) and the 7 model ensembles under a high emissions scenario. Solid lines and shading represent ensemble mean and interdecile spread.

BSO OHT and winter sea ice in the Barents Sea (Fig. 4). The influence of the Fram Strait on sea ice is limited to the northern Greenland Sea in most models.

Under a high emissions scenario, the influence of BSO and Bering Strait OHT expands towards the central Arctic Ocean in the future (2050–2079), consistent with the northward retreat of the sea ice edge. The future influence of the Fram Strait OHT is limited in all models. The expanding influence is generally larger for the Bering Strait OHT on the Pacific side, where it covers parts of the Chukchi Sea, the East Siberian Sea, and the central Arctic Ocean. On the Atlantic side, the expanding influence of the BSO OHT occurs towards the Kara and Laptev Seas. The influence of Bering Strait and BSO OHT thus converge towards the central Arctic Ocean, with models roughly agreeing that the footprints of Atlantic and Pacific OHT (i.e., atlantification and pacification) are separated by the Lomonosov Ridge (see Fig. 1). This border represents the topographically constrained location of the front between the Atlantic and Pacific haloclines (Rudels et al., 1994). Interannual variability in winter sea ice in the Beaufort Sea and areas north of Greenland is largely unaffected by OHT in all models. The projected changes in influence regions for the low emissions scenario are less pronounced than in the high emissions scenario (Fig. S3 in the online supplemental material).

Model differences in the future influence of OHT are larger for the Atlantic side than for the Pacific side. CanESM5 shows the smallest connection between BSO OHT and sea ice on the Atlantic side. EC-Earth3 projects the most pronounced future expansion of atlantification, correlations between sea ice concentration and BSO OHT extending to the central Laptev Sea (Fig. 4e). The strongest future expansion of pacification is projected by the EC-Earth3 and the CESM-LE, where correlations with the Bering Strait OHT extend towards the central Arctic Ocean and the northern Laptev Sea (Fig. 4e,f). The smallest influence region of Bering Strait OHT on the sea ice on the Pacific side is projected by the CanESM5, the GFDL-CM3 and the ACCESS-ESM (Fig. 4c,d,g). It is worth noting that the CanESM5 and the GFDL-CM3 project near ice-free winters across much of the Arctic Ocean. This limits the ability of OHT to influence the ice, simply because there is no ice.

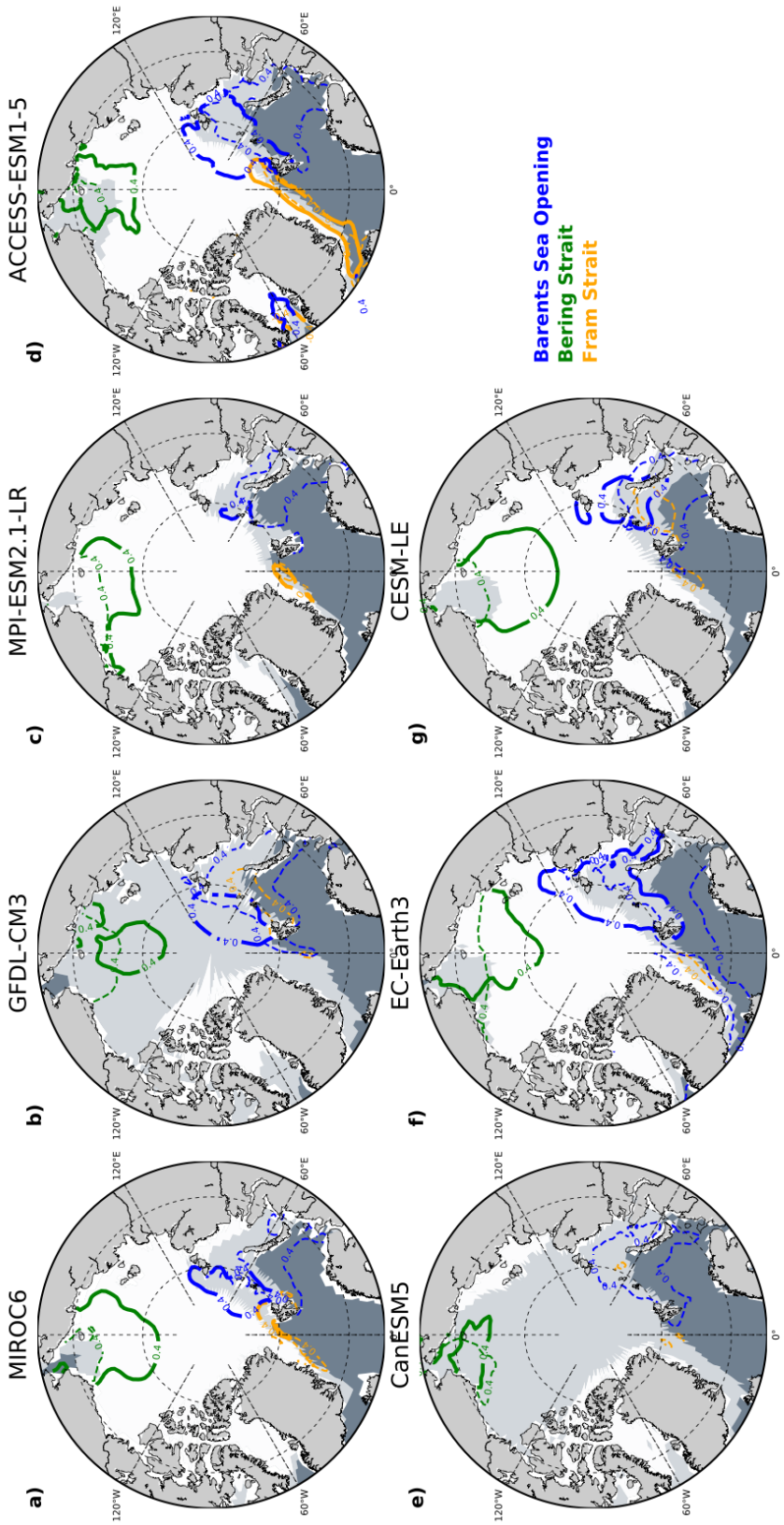

Figure 4. The expanding influence of OHT on winter sea ice concentration. Anomaly correlation (contours; only 0.4 level shown) of winter mean sea ice concentration and OHT through the Fram Strait (yellow), BSO (blue), and Bering Strait (green) for the period 1990–2019 (dashed) and 2050–2079 (solid) under a high emissions scenario for the 7 model ensembles. Background shading shows the ensemble mean winter sea ice edge (based on 50% sea ice concentration for 1990–2019 (gray shading) and 2050–2079 (white shading).

6 Sources of differences in oceanic influence

We now assess possible sources of both, model differences and future changes, in the influence of BSO OHT on the Atlantic side, and Bering Strait OHT on the Pacific side winter sea ice. We represent and quantify the ocean heat transport's systematic impact on winter sea ice area – more ocean heat input, less sea ice - by linear correlation for each of the 60 30-year time periods between 1990–2019 and 2050–2079 for each of the 7 models. This allows us to track changes over time for each model as well as systematic differences between the models. We then relate the degree of impact with the state of its separate parts, sea ice area (Figs. 5a,6a) and heat transport (Figs. 5b,6b), and five other key gateway hydrographic properties as detailed below. Very broadly, the following stand out related to both gateways, across models, and throughout the 21st century. The larger the regional sea ice area, the colder the inflow temperature, the larger the volume transport variability, or the larger the inflow salinity, the tighter the relation between OHT and sea ice area.

We first analyze how the correlation between OHT and winter sea ice is impacted by changes in the mean sea ice area. For the Atlantic side, there is a relationship between the mean sea ice area and the influence of the BSO OHT (Fig. 5a). The smaller the sea ice area, the weaker the influence of OHT. This is consistent with the sea ice edge moving further north (and away from the BSO), thus making the potential influence on winter sea ice smaller. The relationship holds both for the time evolution for each model (quantified by the 30-year running correlations) and for intermodel differences (large markers). For the Pacific side and the Bering Strait OHT (Fig. 6a), there is a similar, albeit weaker, relationship. As the sea ice edge retreats on the Pacific side, large areas see increased winter sea ice variability (Fig. 4), which could increase the influence of the Bering Strait OHT and thus counteract the increased distance of the sea ice edge to the Bering Strait.

We next explore how the connection between OHT and winter sea ice is impacted by the properties of heat transport through the gateways. For the Atlantic side, the connection between OHT and sea ice is not strongly sensitive to differences in mean BSO volume transport (Fig. 5c). We do, however, find that models that overestimate the volume transport *variability* also overestimate the influence of OHT on sea ice (relative to ORAS5; Fig. 5e). All models except the MPI-ESM1-2-LR and the CESM-LE strongly

overestimate the variability, which could be a reason why they simulate a stronger influence of the BSO OHT on the winter sea ice on the Atlantic side. We find that the influence also depends on the mean inflow temperature (Fig. 5d), which is reflected in the mean OHT (Fig. 5b). Higher temperatures (and heat transport) are associated with a weaker influence of BSO OHT on winter sea ice, both for the simulated changes over time for each model, as well as intermodel differences. Part of this correlation stems from the fact that higher average temperatures are associated with lower sea ice area (Fig. 5a). Warmer water at the BSO for the same ice cover could point to more efficient atmospheric cooling in the Barents Sea and thus less influence of OHT. This would for example explain why the MPI-ESM1-2-LR, which has a relatively warm BSO inflow, shows less connection between BSO OHT and sea ice area than models with a similar mean sea ice area.

For the Pacific side, there is a relationship between the volume transport through the Bering Strait and the influence of OHT on winter sea ice (Fig. 6c), which also extends to the volume transport *variability* (Fig. 6e). In models and periods with larger volume transport, the impact of Bering Strait OHT is generally larger. The correlation is even higher if we exclude the Chukchi Sea from the Pacific side region (not shown), indicating that the influence of OHT on regions further into the Arctic tends to be stronger when the volume transport is larger. There is no strong relationship between the mean heat transport and the inflow temperature (and its variability) at the Bering Strait and the connection between OHT and winter sea ice (Fig. 6b,d,f). This indicates that in order to simulate the connection between OHT and sea ice accurately, it is most important that the mean volume transport should be consistent with observational estimates. In ORAS5, the annual mean volume transport through the Bering Strait is 1.3 Sv and the observational estimate is approximately 1.0 Sv (Woodgate, 2018). The EC-Earth3 overestimates and CanESM5 and MPI-ESM1-2-LR underestimate the volume transport through the Bering Strait, and might therefore also over- and underestimate its present and future impact on the winter sea ice area on the Pacific side.

Lastly, we explore the role of the inflow salinity on the impact of OHT on sea ice. Salinity is important in the polar ocean as the main driver of stratification, which can limit how the oceanic heat impacts the sea ice (Polyakov et al., 2018). For the Atlantic side, the influence of the BSO OHT does not depend on the inflow salinity (Fig. 5g). On the Pacific side, however, we find a strong connection with the bottom salinity at the Bering Strait (Fig. 6g), with higher salinity corresponding to a stronger influence of Bering Strait

OHT on winter sea ice. A higher salinity (and thus higher density) inflow of Pacific waters implies less mixing of these waters with the fresher and lighter Polar waters created during ice melt over summer. Fig. 7a-c shows that the Chukchi shelf is stratified in ORAS5 over summer, but only in some models (two are shown here as examples, all are shown in Fig. S4 in the online supplemental material).

Looking at the correlation between winter sea ice and Bering Strait OHT during each month (Fig. 7d), we observe a maximum influence of OHT in early summer along with a second maximum in late autumn. The first maximum represents heat that enters through Bering Strait in summer and re-emerges in autumn and early winter (Serreze et al., 2016), whereas the second maximum is consistent with a more direct impact of inflowing heat on the advancing sea ice in early winter. In the future, the impact of summer heat inflow becomes the primary mode of influence (Fig. 7e), as the winter ice edge moves further away from the Bering Strait. The amount of vertical mixing of the inflowing Pacific water determines how much of its heat mixes with the Polar waters and reaches the surface over summer, where it can be transformed and lose its heat signal until the sea ice advance. Thus, a higher maximum salinity at the Bering Strait is likely a proxy of less vertical mixing and more surface stratification in the Arctic Ocean during summer, facilitating the reemergence of Pacific heat in winter. Indeed, we find that models with higher stratification over the Chukchi shelf simulate a stronger influence of Bering Strait heat transport on winter sea ice (not shown). These are also the models with a higher vertical resolution in the upper 100 m, as indicated in Fig. 7 and Fig. S4 in the online supplemental material.

7 Discussion and Conclusions

The internal variability of the winter Arctic sea ice cover is currently influenced by ocean heat transport into the Arctic Ocean, but it remains uncertain how this influence will change in the future. In this study, we analyzed projected changes in the influence of ocean heat transport on the winter sea ice cover using seven single model large ensembles from CMIP5 and CMIP6. Based on these model projections, we find that the impact of Atlantic and Pacific heat transport will expand in the future. Their respective footprints will divide the Arctic Ocean into two regimes (Richards et al., 2022). Our results suggest that the dividing line for these regimes will be found in the eastern Laptev Sea and along the Lomonosov Ridge, roughly at the front between the Atlantic and Pa-

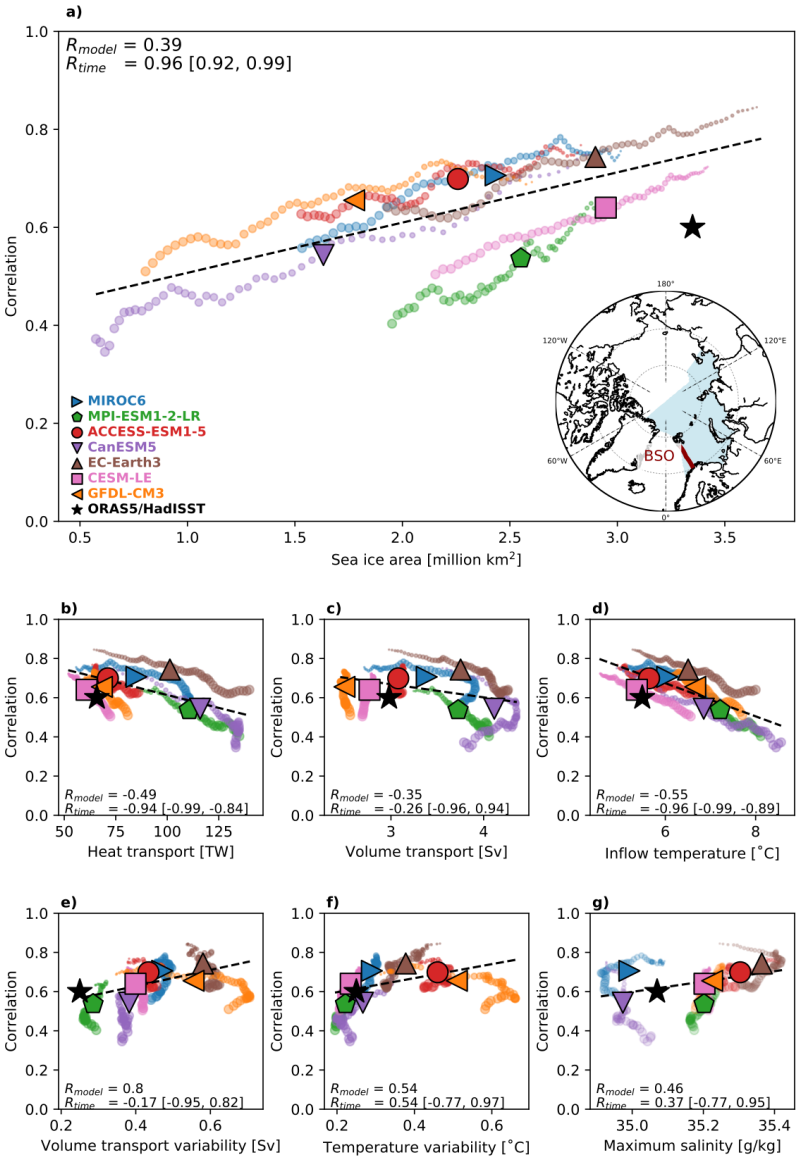

Figure 5. Factors behind differences in the impact of ocean heat transport and winter sea ice on the Atlantic side. Correlation of winter sea ice area on the Atlantic Side (blue shading on map) and annual mean Barents Sea Opening (red line on map) ocean heat transport plotted against the mean a) winter sea ice area, b) ocean heat transport c) volume transport, d) inflow weighted temperature and standard deviation of e) the volume transport and f) inflow weighted temperature, and g) maximum salinity at the gateway for 7 different model ensembles for 60 30-year periods between 1990–2019 and 2050–2079. Light dots indicate values for different periods, large markers indicate a model's average over all periods. Black stars mark estimates based on ORAS5 and HadISST from 1990–2019. Numbers correlation over the models' averages (R_{model}) and over each model's periods (R_{time}), with a range of all models given in brackets. Black dashed lines are linear regressions for all points.

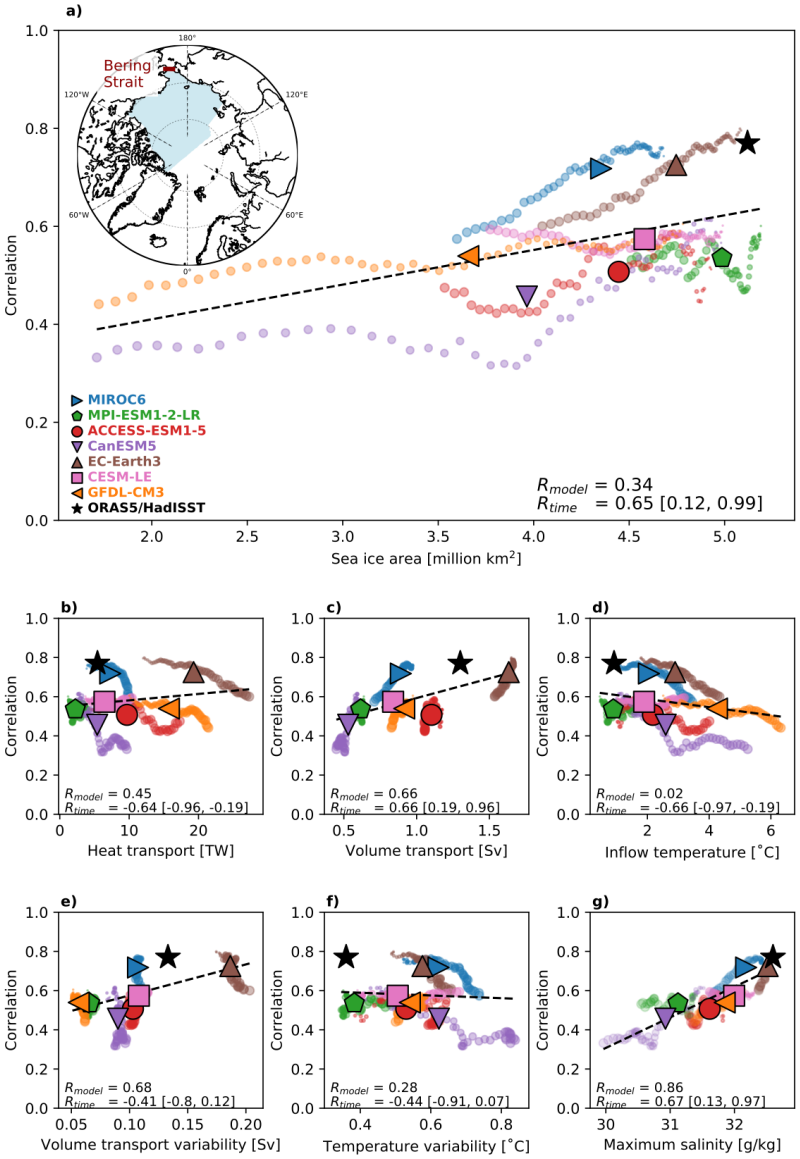

Figure 6. Factors behind differences in the impact of ocean heat transport and winter sea ice on the Pacific side. Same as Fig. 5, but for the Bering Strait ocean heat transport and winter sea ice area on the Pacific side.

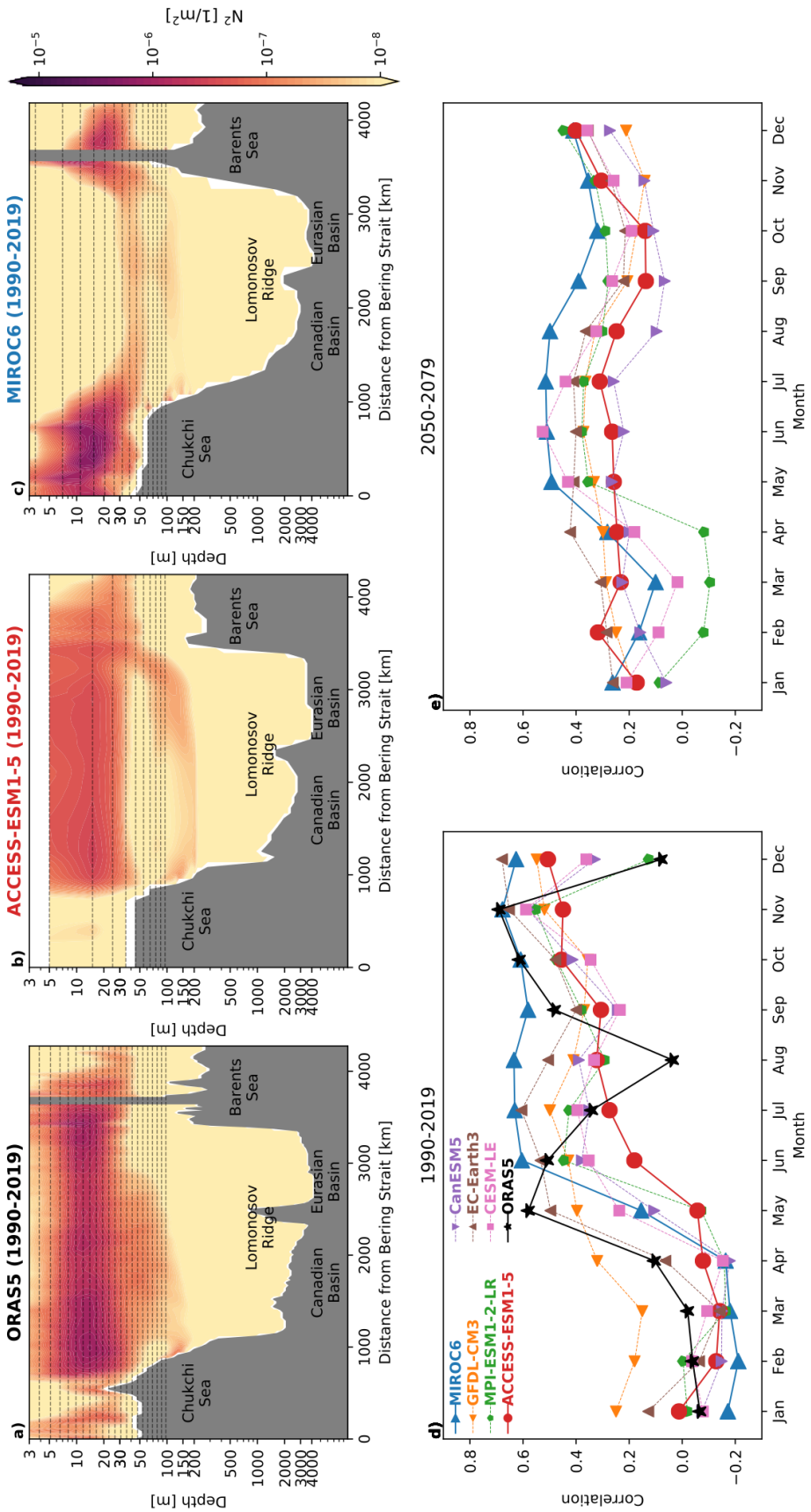

Figure 7. a-c) Vertical section of average August-October vertical stratification (Brunt-Väisälä-Frequency squared) across the Arctic Ocean during 1990–2019 for reanalysis and two models. Horizontal dashed lines indicate the vertical resolution. d-e) Correlation of monthly ocean heat transport through the Bering Strait and the following winter sea ice area on the Pacific side for d) 1990–2019 and e) 2050–2079 under a high emissions scenario.

cific haloclines (Rudels et al., 1994). In agreement with results from CESM-LE (Dörr et al., 2021), the expanding footprint of Atlantic and Pacific ocean heat transport is dominated by the Barents Sea Opening and Bering Strait heat transports, respectively. The direct influence of the Fram Strait heat transport on winter sea ice variability is limited in all models.

Some of the intermodel differences in the changes in strength, location, and timing of the oceanic influence can be traced back to differences in the mean ice state. Especially on the Atlantic side, the influence expands and weakens as the ice edge moves northwards in all models. This means that the future influence of heat transport through the Barents Sea Opening will depend on future sea ice loss. On the Pacific side, the generally weakening influence is offset by its strong regional expansion, and weakening only occurs for a total loss of winter sea ice, something which two models indicate under a strong emissions scenario.

The strength of the future influence is also sensitive to properties at the inflow gateways. On the Atlantic side, most models overestimate the present influence of Barents Sea Opening heat transport because they overestimate its volume transport variability. All models furthermore agree that a future weakening of the Atlantic influence will be driven by the retreat of the sea ice edge and warming of the inflow waters. On the Pacific side, most models underestimate the present influence of Bering Strait heat transport due to a combination of underestimated volume transport and an underestimated summer surface stratification. The future influence depends on how much the oceanic heat entering the central Arctic in early summer can reemerge in autumn and influence the sea ice. Thus, model biases in upper ocean stratification and vertical mixing need to be reduced in order to accurately capture this increasingly important driver of Arctic sea ice variability. These biases could be reduced by increasing the vertical resolution of the upper ocean to properly resolve the shallow summer mixed layer (Rosenblum et al., 2021).

We focused in this study on projected changes under a strong emissions scenario (SSP5-8.5/RCP8.5), but our main conclusions also hold for the low emissions scenario (SSP1-26). The future changes in sea ice are smaller in the low emissions scenario (Fig. S1 in the online supplemental material) and the models show a smaller expansion of the footprints of Atlantic and Pacific heat transport (Fig. S3 in the online supplemental ma-

terial). We find, however, the same sources of model differences as those identified for the high emissions scenario (Figs. 5,6), suggesting that our results are independent of the exact strength of future warming.

The connection between ocean heat transport and sea ice is likely also affected by other factors than those investigated here. The heat transport through the Barents Sea Opening is for example influenced by atmospheric variability over the Nordic Seas (Q. Wang et al., 2019; Madonna & Sandø, 2022). However, we find no relationship between the strength in atmospheric forcing (quantified as the strength of the associated sea level pressure anomaly over Svalbard) and the influence of ocean heat transport on sea ice in the models (not shown). For the Pacific side, differences in the strength of the connection of sea ice to the Bering Strait heat transport could also be related to differences in the simulated pathways of Pacific Water from the Bering Strait towards the central Arctic Ocean. For example, CESM-LE struggles to accurately simulate those pathways (Lavoie et al., 2022), and the same is possibly true for other models.

We focused our analysis on the interannual variability of winter sea ice and OHT. However, OHT also affects internal sea ice variability on longer timescales (Årthun et al., 2019). Internally driven 30-year trends in winter sea ice area on the Atlantic and Pacific sides are significantly correlated to trends in OHT through the BSO and Bering Strait, respectively, for all models (Fig. 8), both now and in the future, although much weaker in the future in some models. The correlations are stronger for the BSO and the Atlantic side, and for the recent past. For externally driven trends (comparing ensemble mean trends), there is a strong connection for the Atlantic side, weakening in the future, but a much weaker connection for the Pacific side. This suggests that the long-term (externally forced) increase in oceanic heat input is a major driver for the sea ice loss on the Atlantic side, but not the main driver on the Pacific side.

To identify sources of model uncertainty in future sea ice projections, several studies have sought after emergent constraints, which are simple relationships between sea ice loss and mean quantities that are valid in a large range of models and observations (Mahlstein & Knutti, 2012; Massonnet et al., 2012, 2018; Horvat, 2021). Instead of constraining sea ice projections, where ocean heat transport is often used as a constraining variable, here we tried to constrain the future role of ocean heat transport itself. We find that the identified relationships are independent of horizontal model resolution (Table

1), consistent with the findings of Docquier et al. (2020) on the impact of ocean heat transport on the Atlantic side. The vertical resolution may however play a role as discussed above. Besides identifying the constraining factors, a result of our study is that the factors on the Pacific side are different from the ones on the Atlantic side. The expanding influence of Atlantic and Pacific heat on winter sea ice can be seen as tracers of the atlantification and pacification of the upper Arctic Ocean, which has important consequences for the Arctic ecosystem (Polyakov et al., 2020; Ingvaldsen et al., 2021). Our study highlights the processes that have to be improved in current climate models in order to capture the expanding influence of ocean heat transport on the future Arctic winter sea ice cover.

Acknowledgments

All authors were funded by the Research Council of Norway projects Nansen Legacy (Grant 276730) and the Trond Mohn Foundation (Grant BFS2018TMT01). We acknowledge the World Climate Research Programme, which, through its Working Group on Coupled Modelling, coordinated and promoted CMIP6. We thank the climate modeling groups for producing and making available their model output, the Earth System Grid Federation (ESGF) for archiving the data and providing access, and the multiple funding agencies who support CMIP6 and ESGF. We thank the US CLIVAR Working Group on Large Ensembles for providing large ensemble output via the Multi-Model Large Ensemble Archive. Furthermore, we thank the CESM Large Ensemble Community Project for making their data publicly accessible.

All data in this study are publicly available. Output from ERA5 and ORAS5 are available through the Copernicus Climate Change Service's Climate Data Store (`https://cds.climate.copernicus.eu/cdsapp#!/home`). Output from the CMIP6 models MPI-ESM1-2-LR, MIROC6, CanESM5, EC-Earth3 and ACCESS-ESM1-5 are available via the Earth System Grid Federation's CMIP6 archive (`https://esgf-node.llnl.gov/projects/cmip6/`). Output from CESM-LE's high warming and low warming runs is available via the Earth System Grid: (`https://www.earthsystemgrid.org`). Output from the GFDL-CM3-LENS is available through the Multi-Model Large Ensemble Archive (`https://www.earthsystemgrid.org/dataset/ucar.cgd.ccsm4.CLIVAR_LE.html`). Observed sea ice concentration from HadISST2 is available through the UK Met Office website (`https://www.metoffice.gov.uk/hadobs/hadisst2/data/download.html`).

References

Årthun, M., Eldevik, T., & Smedsrud, L. H. (2019, March). The Role of Atlantic Heat Transport in Future Arctic Winter Sea Ice Loss. *Journal of Climate*, *32*(11), 3327–3341. doi: 10.1175/JCLI-D-18-0750.1

Årthun, M., Eldevik, T., Smedsrud, L. H., Skagseth, Ø., & Ingvaldsen, R. B. (2012, July). Quantifying the Influence of Atlantic Heat on Barents Sea Ice Variability and Retreat. *Journal of Climate*, *25*(13), 4736–4743. doi: 10.1175/JCLI-D-11-00466.1

Årthun, M., Onarheim, I. H., Dörr, J., & Eldevik, T. (2021). The Seasonal and Regional Transition to an Ice-Free Arctic. *Geophysical Research Letters*, *48*(1),

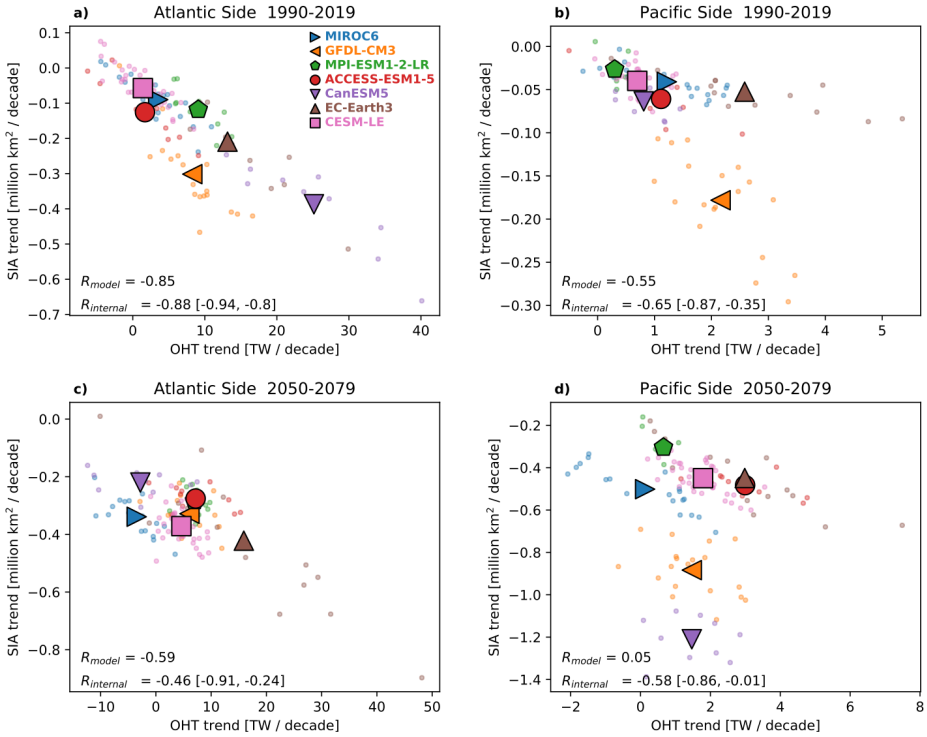

Figure 8. Scatter plot of 30-year trends in winter sea ice area for a,c) the Atlantic side and b,d) Pacific side against 30-year trends in the ocean heat transport (OHT) through a,c) the Barents Sea Opening and b,d) the Bering Strait for a,b) 1990–2019 and c,d) 2059–2079. Light dots represent single members, large markers indicate each model's ensemble mean. Correlations figures are over the models' averages (R_{model}) and the mean correlation over each model's ensemble members ($R_{internal}$), with a range of all models given in brackets.

e2020GL090825. doi: 10.1029/2020GL090825

Beszczynska-Möller, A., Fahrbach, E., Schauer, U., & Hansen, E. (2012, July). Variability in Atlantic water temperature and transport at the entrance to the Arctic Ocean, 1997–2010. *ICES Journal of Marine Science*, *69*(5), 852–863. doi: 10.1093/icesjms/fss056

Carmack, E., Polyakov, I., Padman, L., Fer, I., Hunke, E., Hutchings, J., ... Winsor, P. (2015, December). Toward Quantifying the Increasing Role of Oceanic Heat in Sea Ice Loss in the New Arctic. *Bulletin of the American Meteorological Society*, *96*(12), 2079–2105. doi: 10.1175/BAMS-D-13-00177.1

Community, S. (2020). Arctic Sea Ice in CMIP6. *Geophysical Research Letters*, *47*(10), e2019GL086749. doi: 10.1029/2019GL086749

Deser, C., Lehner, F., Rodgers, K. B., Ault, T., Delworth, T. L., DiNezio, P. N., ... Ting, M. (2020, April). Insights from Earth system model initial-condition large ensembles and future prospects. *Nature Climate Change*, *10*(4), 277–286. doi: 10.1038/s41558-020-0731-2

Docquier, D., Fuentes-Franco, R., Koenigk, T., & Fichefet, T. (2020). Sea Ice—Ocean Interactions in the Barents Sea Modeled at Different Resolutions. *Frontiers in Earth Science*, *8*. doi: 10.3389/feart.2020.00172

Docquier, D., & Königk, T. (2021). A review of interactions between ocean heat transport and Arctic sea ice. *Environmental Research Letters*. doi: 10.1088/1748-9326/ac30be

Dörr, J., Årthun, M., Eldevik, T., & Madonna, E. (2021, November). Mechanisms of Regional Winter Sea-Ice Variability in a Warming Arctic. *Journal of Climate*, *34*(21), 8635–8653. doi: 10.1175/JCLI-D-21-0149.1

Döscher, R., Acosta, M., Alessandri, A., Anthoni, P., Arneth, A., Arsouze, T., ... Zhang, Q. (2021, February). The EC-Earth3 Earth System Model for the Climate Model Intercomparison Project 6. *Geoscientific Model Development Discussions*, 1–90. doi: 10.5194/gmd-2020-446

England, M., Jahn, A., & Polvani, L. (2019, July). Nonuniform Contribution of Internal Variability to Recent Arctic Sea Ice Loss. *Journal of Climate*, *32*(13), 4039–4053. doi: 10.1175/JCLI-D-18-0864.1

Eyring, V., Bony, S., Meehl, G. A., Senior, C. A., Stevens, B., Stouffer, R. J., & Taylor, K. E. (2016, May). Overview of the Coupled Model Intercomparison

Project Phase 6 (CMIP6) experimental design and organization. *Geoscientific Model Development*, *9*(5), 1937–1958. doi: 10.5194/gmd-9-1937-2016

Horvat, C. (2021, April). Marginal ice zone fraction benchmarks sea ice and climate model skill. *Nature Communications*, *12*(1), 2221. doi: 10.1038/s41467-021-22004-7

Ingvaldsen, R. B., Assmann, K. M., Primicerio, R., Fossheim, M., Polyakov, I. V., & Dolgov, A. V. (2021, December). Physical manifestations and ecological implications of Arctic Atlantification. *Nature Reviews Earth & Environment*, *2*(12), 874–889. doi: 10.1038/s43017-021-00228-x

Kay, J. E., Deser, C., Phillips, A., Mai, A., Hannay, C., Strand, G., ... Vertenstein, M. (2015, August). The Community Earth System Model (CESM) Large Ensemble Project: A Community Resource for Studying Climate Change in the Presence of Internal Climate Variability. *Bulletin of the American Meteorological Society*, *96*(8), 1333–1349. doi: 10.1175/BAMS-D-13-00255.1

Lavoie, J., Tremblay, B., & Rosenblum, E. (2022). Pacific Waters Pathways and Vertical Mixing in the CESM1-LE: Implication for Mixed Layer Depth Evolution and Sea Ice Mass Balance in the Canada Basin. *Journal of Geophysical Research: Oceans*, *127*(2), e2021JC017729. doi: 10.1029/2021JC017729

Li, Z., Ding, Q., Steele, M., & Schweiger, A. (2022, January). Recent upper Arctic Ocean warming expedited by summertime atmospheric processes. *Nature Communications*, *13*(1), 362. doi: 10.1038/s41467-022-28047-8

Lind, S., Ingvaldsen, R. B., & Furevik, T. (2018, July). Arctic warming hotspot in the northern Barents Sea linked to declining sea-ice import. *Nature Climate Change*, *8*(7), 634–639. doi: 10.1038/s41558-018-0205-y

Lundesgaard, Ø., Sundfjord, A., & Renner, A. H. H. (2021). Drivers of Interannual Sea Ice Concentration Variability in the Atlantic Water Inflow Region North of Svalbard. *Journal of Geophysical Research: Oceans*, *126*(4), e2020JC016522. doi: 10.1029/2020JC016522

Madonna, E., & Sandø, A. B. (2022). Understanding Differences in North Atlantic Poleward Ocean Heat Transport and Its Variability in Global Climate Models. *Geophysical Research Letters*, *49*(1), e2021GL096683. doi: 10.1029/2021GL096683

Mahlstein, I., & Knutti, R. (2012). September Arctic sea ice predicted to disappear

near 2°C global warming above present. *Journal of Geophysical Research: Atmospheres*, *117*(D6). doi: 10.1029/2011JD016709

Massonnet, F., Fichefet, T., Goosse, H., Bitz, C. M., Philippon-Berthier, G., Holland, M. M., & Barriat, P.-Y. (2012, November). Constraining projections of summer Arctic sea ice. *The Cryosphere*, *6*(6), 1383–1394. doi: 10.5194/tc-6-1383-2012

Massonnet, F., Vancoppenolle, M., Goosse, H., Docquier, D., Fichefet, T., & Blanchard-Wrigglesworth, E. (2018, July). Arctic sea-ice change tied to its mean state through thermodynamic processes. *Nature Climate Change*, *8*(7), 599–603. doi: 10.1038/s41558-018-0204-z

Mauritsen, T., Bader, J., Becker, T., Behrens, J., Bittner, M., Brokopf, R., ... Roeckner, E. (2019). Developments in the MPI-M Earth System Model version 1.2 (MPI-ESM1.2) and Its Response to Increasing CO2. *Journal of Advances in Modeling Earth Systems*, *11*(4), 998–1038. doi: 10.1029/2018MS001400

Milinski, S., Maher, N., & Olonscheck, D. (2020, October). How large does a large ensemble need to be? *Earth System Dynamics*, *11*(4), 885–901. doi: 10.5194/esd-11-885-2020

Polyakov, I., Alkire, M. B., Bluhm, B. A., Brown, K. A., Carmack, E. C., Chierici, M., ... Wassmann, P. (2020). Borealization of the Arctic Ocean in Response to Anomalous Advection From Sub-Arctic Seas. *Frontiers in Marine Science*, *7*. doi: 10.3389/fmars.2020.00491

Polyakov, I., Pnyushkov, A., & Carmack, E. (2018, October). Stability of the arctic halocline: A new indicator of arctic climate change. *Environmental Research Letters*, *13*. doi: 10.1088/1748-9326/aaec1e

Polyakov, I., Pnyushkov, A. V., Alkire, M. B., Ashik, I. M., Baumann, T. M., Carmack, E. C., ... Yulin, A. (2017, April). Greater role for Atlantic inflows on sea-ice loss in the Eurasian Basin of the Arctic Ocean. *Science*, *356*(6335), 285–291. doi: 10.1126/science.aai8204

Rawlins, M. A., Steele, M., Holland, M. M., Adam, J. C., Cherry, J. E., Francis, J. A., ... Zhang, T. (2010, November). Analysis of the Arctic System for Freshwater Cycle Intensification: Observations and Expectations. *Journal of Climate*, *23*(21), 5715–5737. doi: 10.1175/2010JCLI3421.1

Richards, A. E., Johnson, H. L., & Lique, C. (2022). Spatial and temporal vari-

ability of Atlantic Water in the Arctic from forty years of observations. *Journal of Geophysical Research: Oceans*, *n/a*(n/a), e2021JC018358. doi: 10.1029/2021JC018358

Rosenblum, E., Fajber, R., Stroeve, J. C., Gille, S. T., Tremblay, L. B., & Carmack, E. C. (2021). Surface Salinity Under Transitioning Ice Cover in the Canada Basin: Climate Model Biases Linked to Vertical Distribution of Fresh Water. *Geophysical Research Letters*, *48*(21), e2021GL094739. doi: 10.1029/2021GL094739

Rudels, B., Jones, E. P., Anderson, L. G., & Kattner, G. (1994). On the Intermediate Depth Waters of the Arctic Ocean. In *The Polar Oceans and Their Role in Shaping the Global Environment* (pp. 33–46). American Geophysical Union (AGU). doi: 10.1029/GM085p0033

Rudels, B., Korhonen, M., Schauer, U., Pisarev, S., Rabe, B., & Wisotzki, A. (2015, March). Circulation and transformation of Atlantic water in the Eurasian Basin and the contribution of the Fram Strait inflow branch to the Arctic Ocean heat budget. *Progress in Oceanography*, *132*, 128–152. doi: 10.1016/j.pocean.2014.04.003

Sanderson, B. M., Xu, Y., Tebaldi, C., Wehner, M., O'Neill, B., Jahn, A., ... Lamarque, J. F. (2017, September). Community climate simulations to assess avoided impacts in 1.5 and 2 °C futures. *Earth System Dynamics*, *8*(3), 827–847. doi: 10.5194/esd-8-827-2017

Schlichtholz, P. (2011). Influence of oceanic heat variability on sea ice anomalies in the Nordic Seas. *Geophysical Research Letters*, *38*(5). doi: 10.1029/2010GL045894

Serreze, M. C., Barrett, A. P., Crawford, A. D., & Woodgate, R. A. (2019). Monthly Variability in Bering Strait Oceanic Volume and Heat Transports, Links to Atmospheric Circulation and Ocean Temperature, and Implications for Sea Ice Conditions. *Journal of Geophysical Research: Oceans*, *n/a*(n/a). doi: 10.1029/2019JC015422

Serreze, M. C., Crawford, A. D., Stroeve, J. C., Barrett, A. P., & Woodgate, R. A. (2016). Variability, trends, and predictability of seasonal sea ice retreat and advance in the Chukchi Sea. *Journal of Geophysical Research: Oceans*, *121*(10), 7308–7325. doi: 10.1002/2016JC011977

Shu, Q., Wang, Q., Song, Z., & Qiao, F. (2021, May). The poleward enhanced Arctic Ocean cooling machine in a warming climate. *Nature Communications*, *12*(1), 2966. doi: 10.1038/s41467-021-23321-7

Skagseth, Ø., Eldevik, T., Årthun, M., Asbjørnsen, H., Lien, V. S., & Smedsrud, L. H. (2020, July). Reduced efficiency of the Barents Sea cooling machine. *Nature Climate Change*, *10*(7), 661–666. doi: 10.1038/s41558-020-0772-6

Sun, L., Alexander, M., & Deser, C. (2018). Evolution of the Global Coupled Climate Response to Arctic Sea Ice Loss during 1990–2090 and Its Contribution to Climate Change. *Journal of Climate*, *31*(19), 7823–7843.

Swart, N. C., Cole, J. N. S., Kharin, V. V., Lazare, M., Scinocca, J. F., Gillett, N. P., ... Winter, B. (2019, November). The Canadian Earth System Model version 5 (CanESM5.0.3). *Geoscientific Model Development*, *12*(11), 4823–4873. doi: 10.5194/gmd-12-4823-2019

Tatebe, H., Ogura, T., Nitta, T., Komuro, Y., Ogochi, K., Takemura, T., ... Kimoto, M. (2019, July). Description and basic evaluation of simulated mean state, internal variability, and climate sensitivity in MIROC6. *Geoscientific Model Development*, *12*(7), 2727–2765. doi: 10.5194/gmd-12-2727-2019

Titchner, H. A., & Rayner, N. A. (2014). The Met Office Hadley Centre sea ice and sea surface temperature data set, version 2: 1. Sea ice concentrations. *Journal of Geophysical Research: Atmospheres*, *119*(6), 2864–2889. doi: 10.1002/2013JD020316

Wang, Q., Wang, X., Wekerle, C., Danilov, S., Jung, T., Koldunov, N., ... Sidorenko, D. (2019). Ocean Heat Transport Into the Barents Sea: Distinct Controls on the Upward Trend and Interannual Variability. *Geophysical Research Letters*, *46*(22), 13180–13190. doi: 10.1029/2019GL083837

Wang, Y., Liu, N., & Zhang, Z. (2021). Sea Ice Reduction During Winter of 2017 Due to Oceanic Heat Supplied by Pacific Water in the Chukchi Sea, West Arctic Ocean. *Frontiers in Marine Science*, *8*, 595. doi: 10.3389/fmars.2021.650909

Woodgate, R. A. (2018, January). Increases in the Pacific inflow to the Arctic from 1990 to 2015, and insights into seasonal trends and driving mechanisms from year-round Bering Strait mooring data. *Progress in Oceanography*, *160*, 124–154. doi: 10.1016/j.pocean.2017.12.007

Ziehn, T., Chamberlain, M. A., Law, R. M., Lenton, A., Bodman, R. W., Dix, M., ... Srbinovsky, J. (2020). The Australian Earth System Model: ACCESS-ESM1.5. *Journal of Southern Hemisphere Earth Systems Science*, *70*(1), 193. doi: 10.1071/ES19035

Zuo, H., Balmaseda, M. A., Tietsche, S., Mogensen, K., & Mayer, M. (2019, June). The ECMWF operational ensemble reanalysis–analysis system for ocean and sea ice: A description of the system and assessment. *Ocean Science*, *15*(3), 779–808. doi: 10.5194/os-15-779-2019

Figure 1.

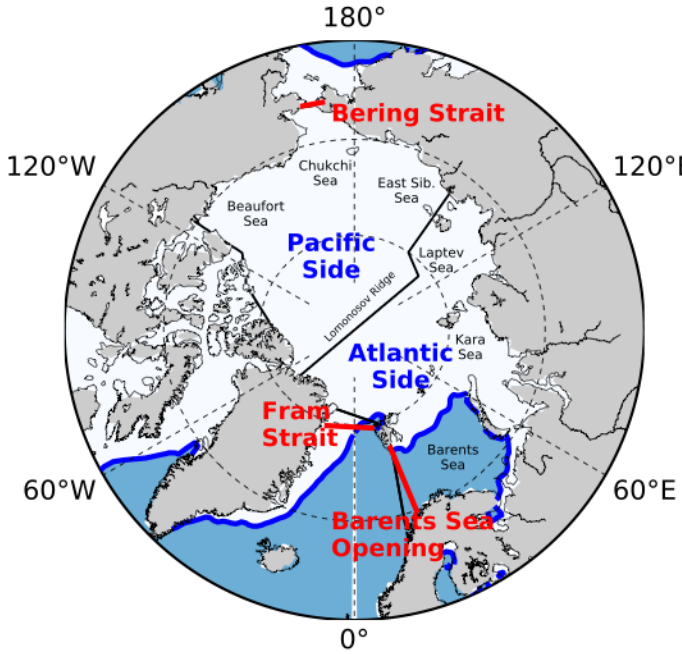
180°
120°W
120°E
60°W
60°E
0°
Bering Strait
Chukchi Sea
East Sib. Sea
Beaufort Sea
Pacific Side
Laptev Sea
Lomonosov Ridge
Kara Sea
Atlantic Side
Fram Strait
Barents Sea
Barents Sea Opening

Figure 2.

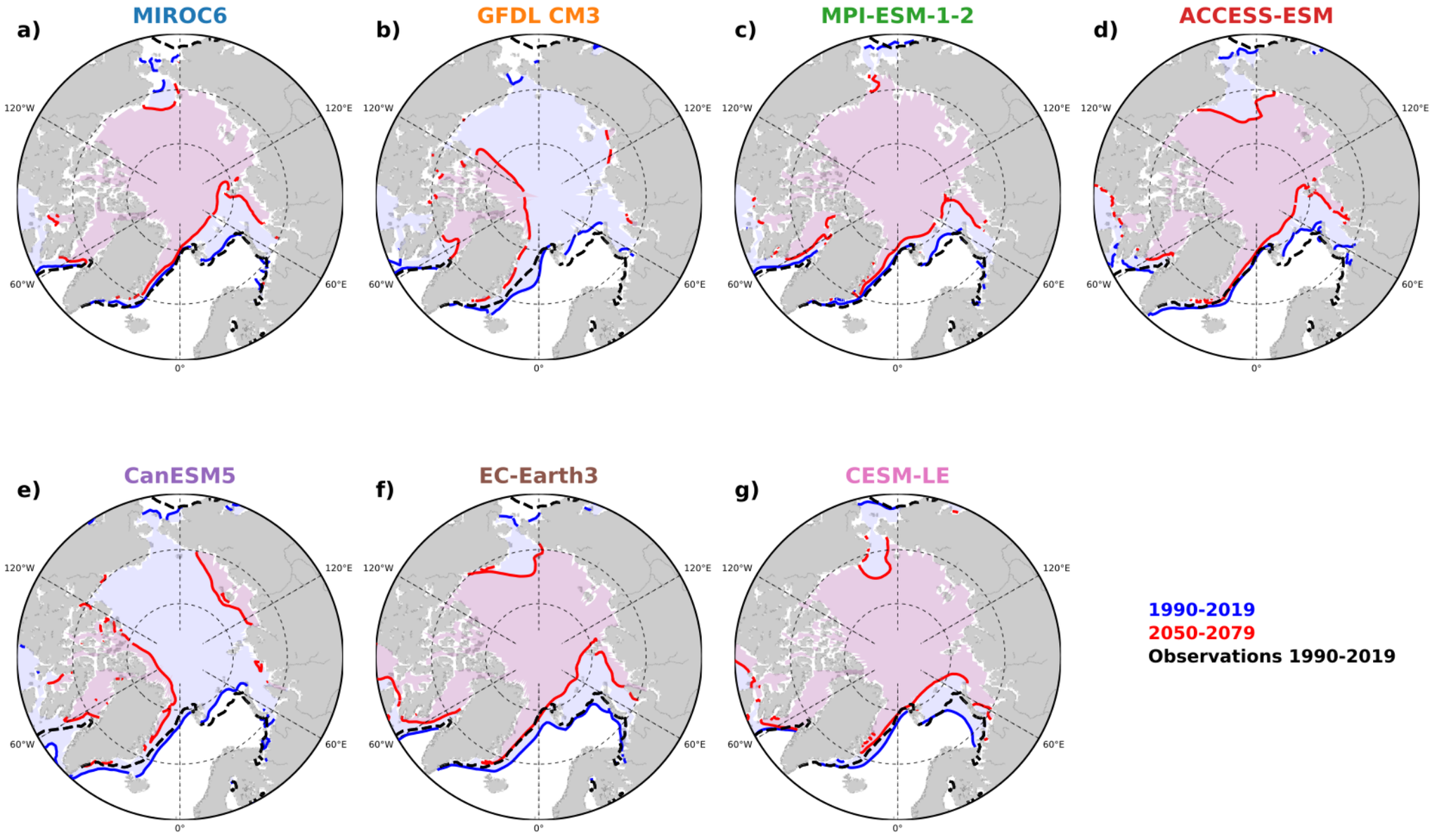
a)
MIROC6
b)
GFDL CM3
c)
MPI-ESM-1-2
d)
ACCESS-ESM
e)
CanESM5
f)
EC-Earth3
g)
CESM-LE
120°W
120°E
60°W
60°E
0°
1990-2019
2050-2079
Observations 1990-2019

Figure 3.

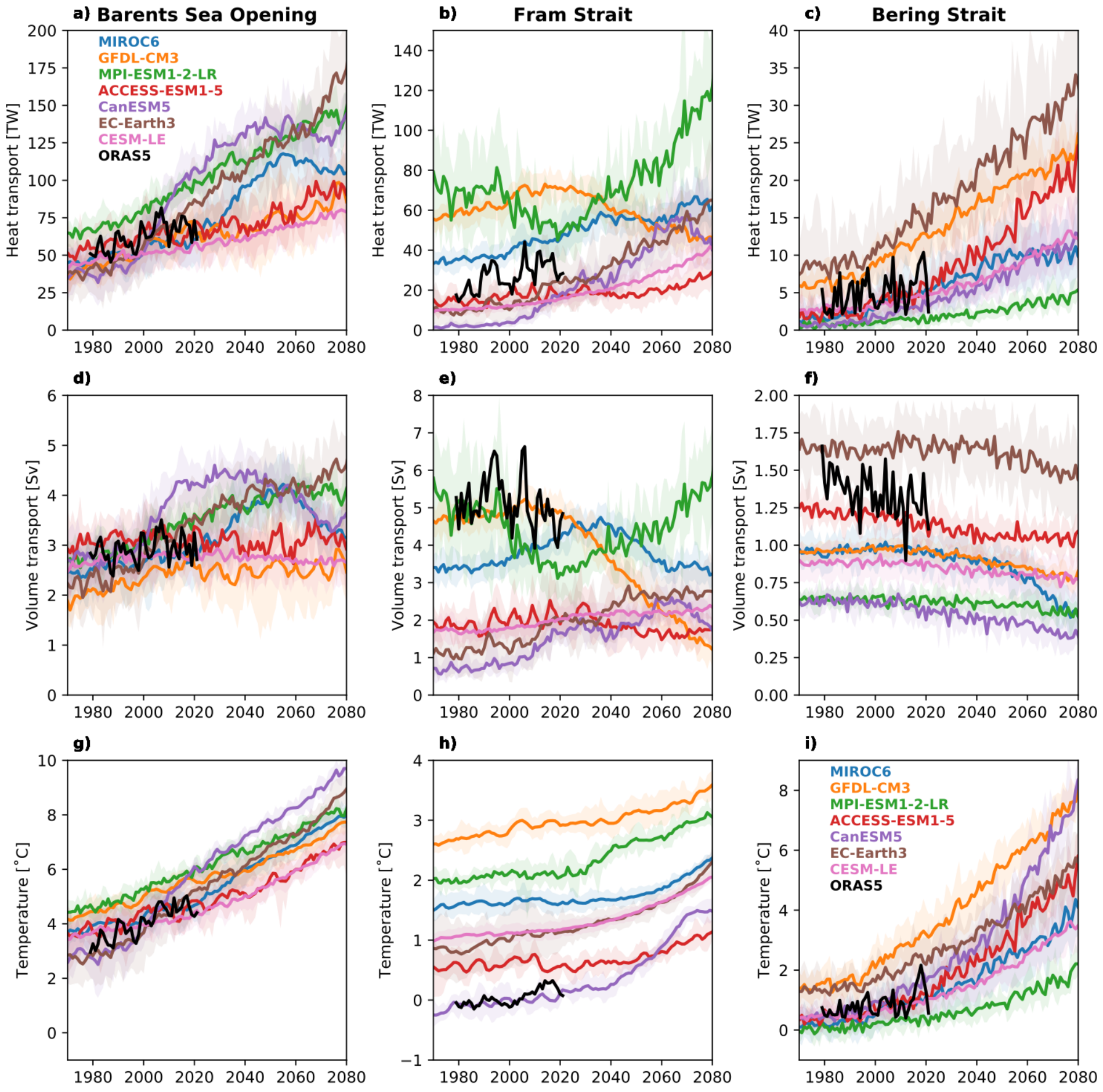
a) Barents Sea Opening
b) Fram Strait
c) Bering Strait
d)
e)
f)
g)
h)
i)
MIROC6
GFDL-CM3
MPI-ESM1-2-LR
ACCESS-ESM1-5
CanESM5
EC-Earth3
CESM-LE
ORAS5
Heat transport [TW]
Volume transport [Sv]
Temperature [˚C]
1980
2000
2020
2040
2060
2080

Figure 4.

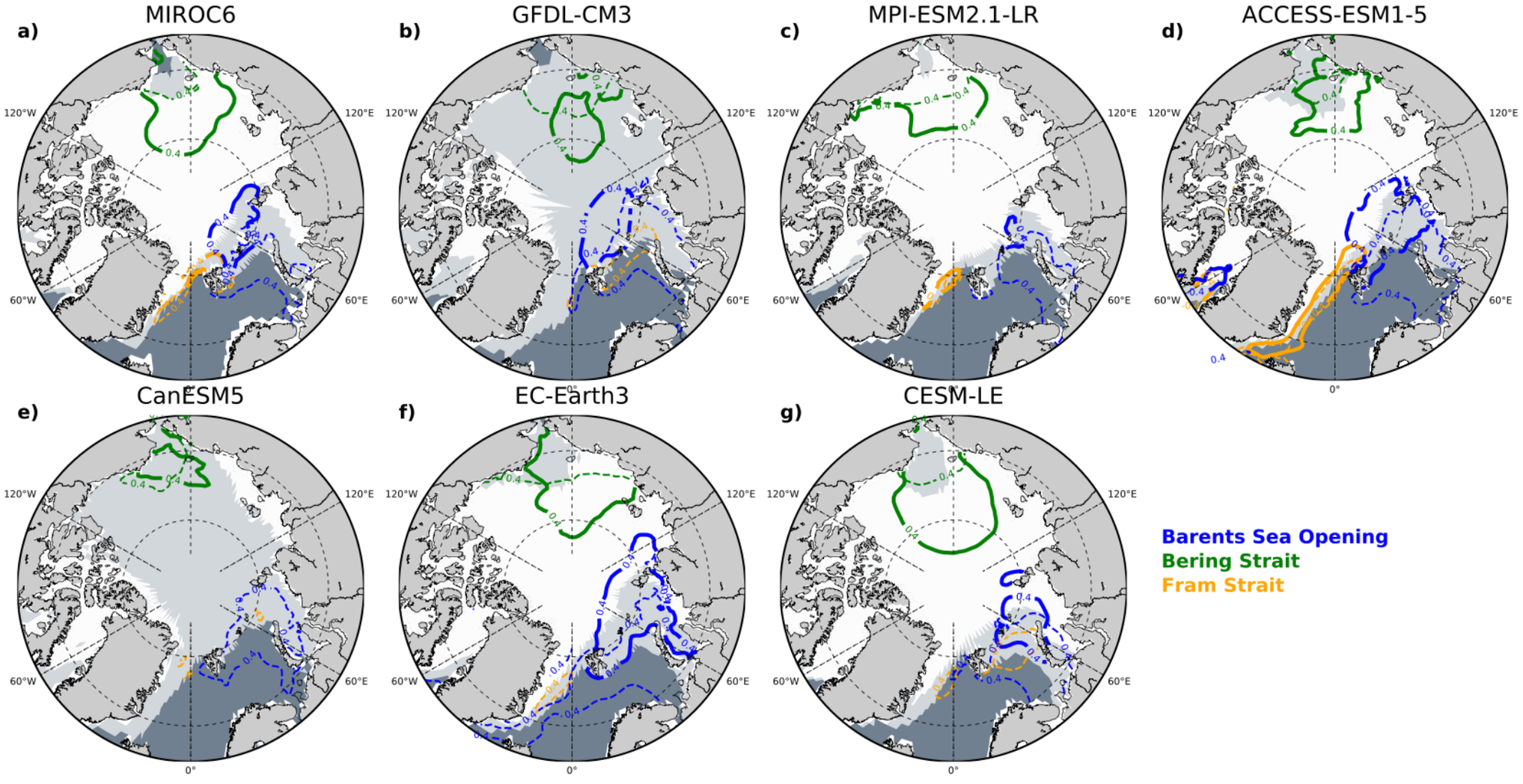
a)
MIROC6
b)
GFDL-CM3
c)
MPI-ESM2.1-LR
d)
ACCESS-ESM1-5
e)
CanESM5
f)
EC-Earth3
g)
CESM-LE
120°W
120°E
60°W
60°E
0°
0.4
Barents Sea Opening
Bering Strait
Fram Strait

Figure 5.

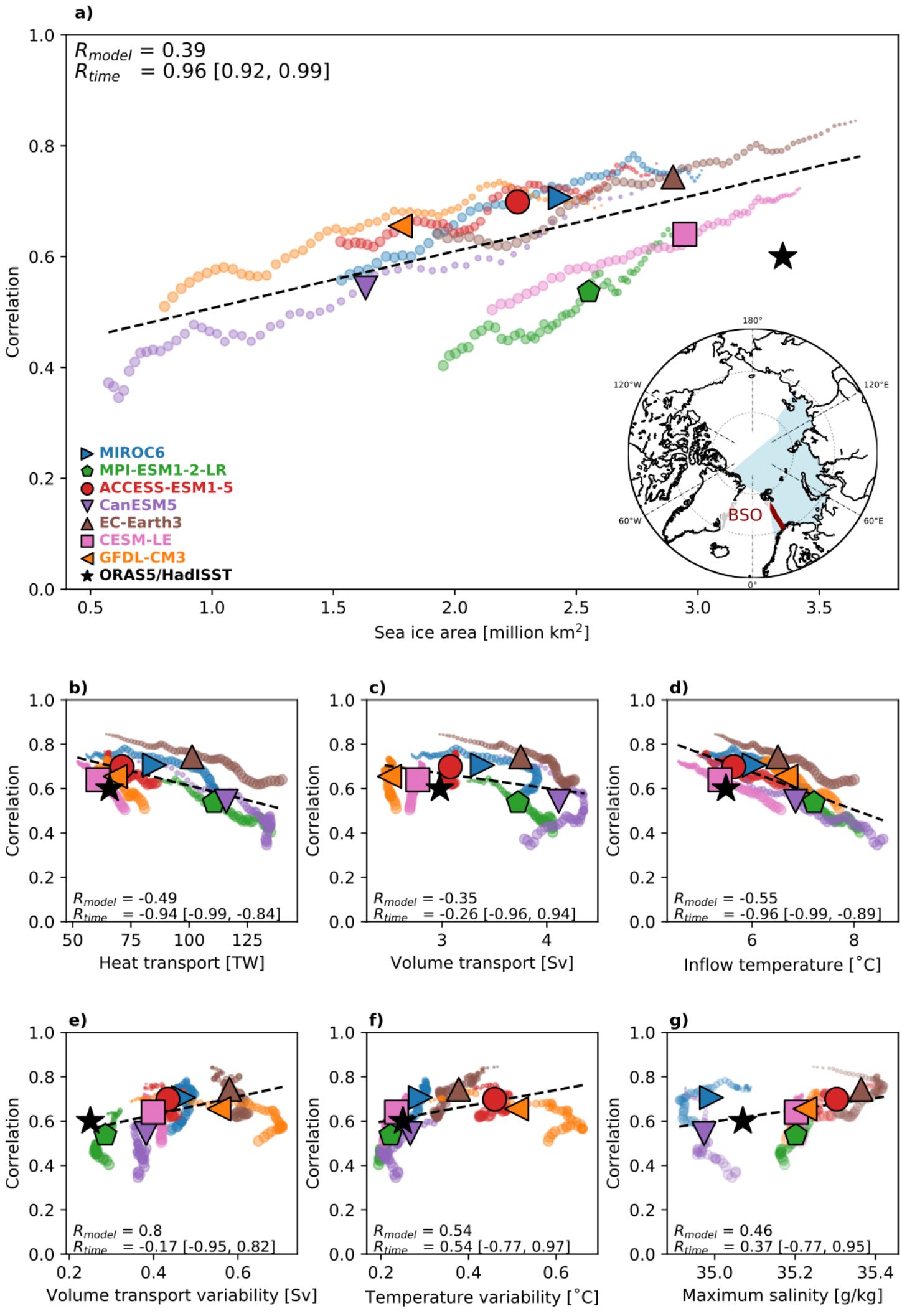
a)
R_{model} = 0.39
R_{time} = 0.96 [0.92, 0.99]
Correlation
Sea ice area [million km^2]
MIROC6
MPI-ESM1-2-LR
ACCESS-ESM1-5
CanESM5
EC-Earth3
CESM-LE
GFDL-CM3
ORAS5/HadISST
BSO
180°
120°W
120°E
60°W
60°E
0°
b)
R_{model} = -0.49
R_{time} = -0.94 [-0.99, -0.84]
Heat transport [TW]
c)
R_{model} = -0.35
R_{time} = -0.26 [-0.96, 0.94]
Volume transport [Sv]
d)
R_{model} = -0.55
R_{time} = -0.96 [-0.99, -0.89]
Inflow temperature [˚C]
e)
R_{model} = 0.8
R_{time} = -0.17 [-0.95, 0.82]
Volume transport variability [Sv]
f)
R_{model} = 0.54
R_{time} = 0.54 [-0.77, 0.97]
Temperature variability [˚C]
g)
R_{model} = 0.46
R_{time} = 0.37 [-0.77, 0.95]
Maximum salinity [g/kg]

Figure 6.

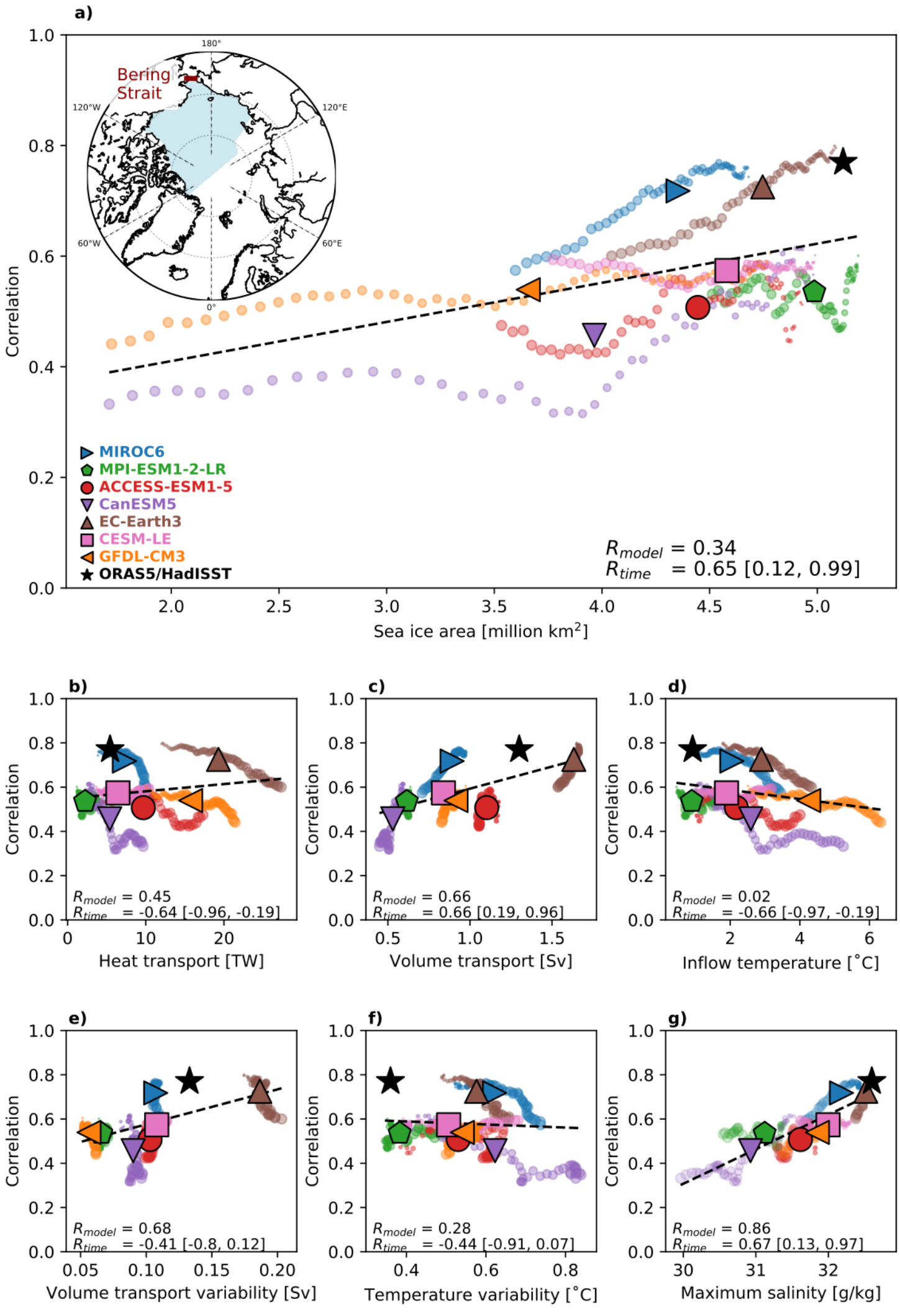
a)
Bering Strait
180°
120°W
120°E
60°W
60°E
0°
Correlation
Sea ice area [million km^2]
MIROC6
MPI-ESM1-2-LR
ACCESS-ESM1-5
CanESM5
EC-Earth3
CESM-LE
GFDL-CM3
ORAS5/HadISST
R_{model} = 0.34
R_{time} = 0.65 [0.12, 0.99]
b)
Heat transport [TW]
R_{model} = 0.45
R_{time} = -0.64 [-0.96, -0.19]
c)
Volume transport [Sv]
R_{model} = 0.66
R_{time} = 0.66 [0.19, 0.96]
d)
Inflow temperature [˚C]
R_{model} = 0.02
R_{time} = -0.66 [-0.97, -0.19]
e)
Volume transport variability [Sv]
R_{model} = 0.68
R_{time} = -0.41 [-0.8, 0.12]
f)
Temperature variability [˚C]
R_{model} = 0.28
R_{time} = -0.44 [-0.91, 0.07]
g)
Maximum salinity [g/kg]
R_{model} = 0.86
R_{time} = 0.67 [0.13, 0.97]

Figure 7.

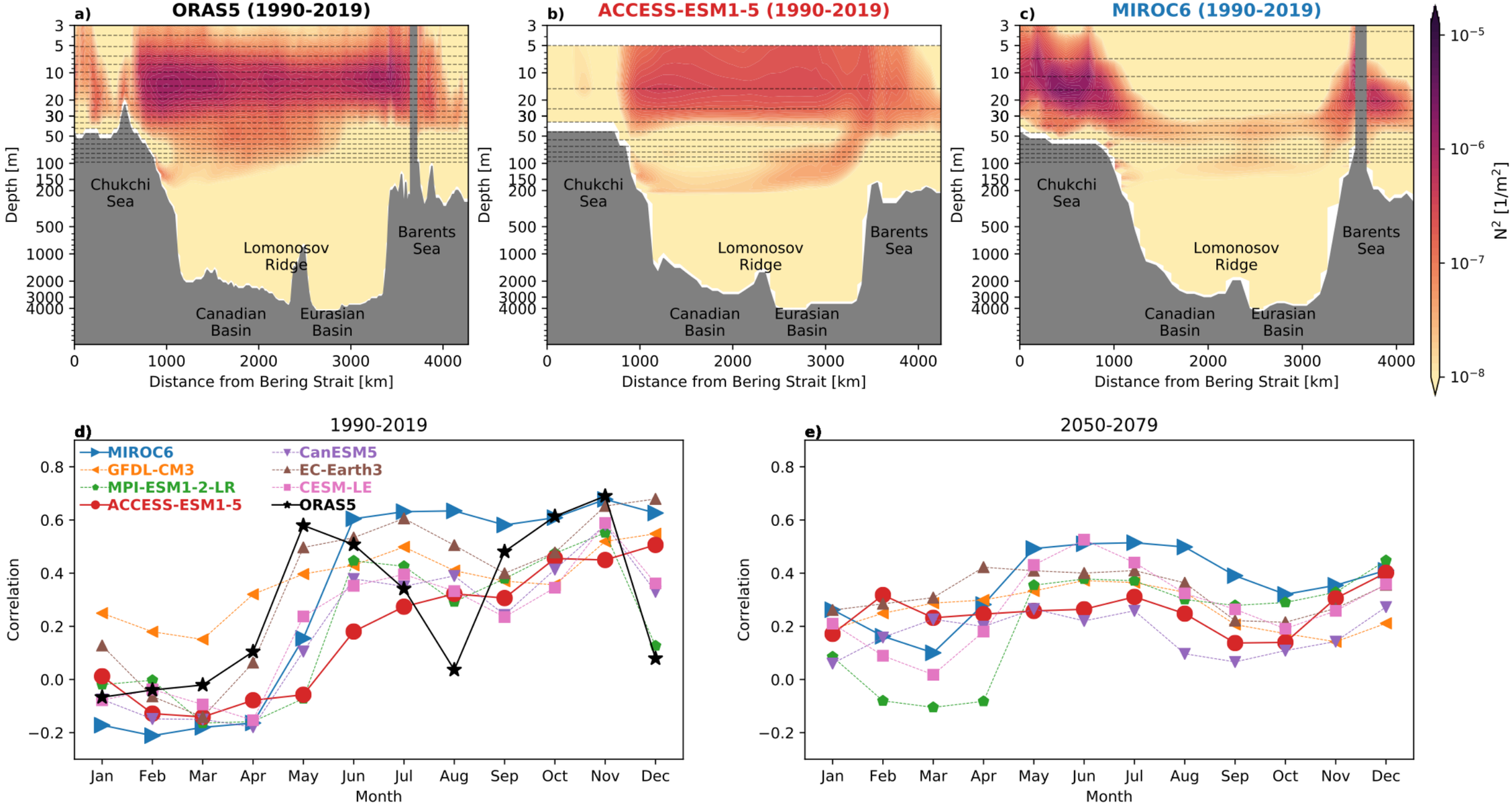
a)
ORAS5 (1990-2019)
b)
ACCESS-ESM1-5 (1990-2019)
c)
MIROC6 (1990-2019)
Depth [m]
Distance from Bering Strait [km]
Chukchi Sea
Lomonosov Ridge
Barents Sea
Canadian Basin
Eurasian Basin
N² [1/m²]
d)
1990-2019
e)
2050-2079
MIROC6
GFDL-CM3
MPI-ESM1-2-LR
ACCESS-ESM1-5
CanESM5
EC-Earth3
CESM-LE
ORAS5
Correlation
Month
Jan
Feb
Mar
Apr
May
Jun
Jul
Aug
Sep
Oct
Nov
Dec

Figure 8.

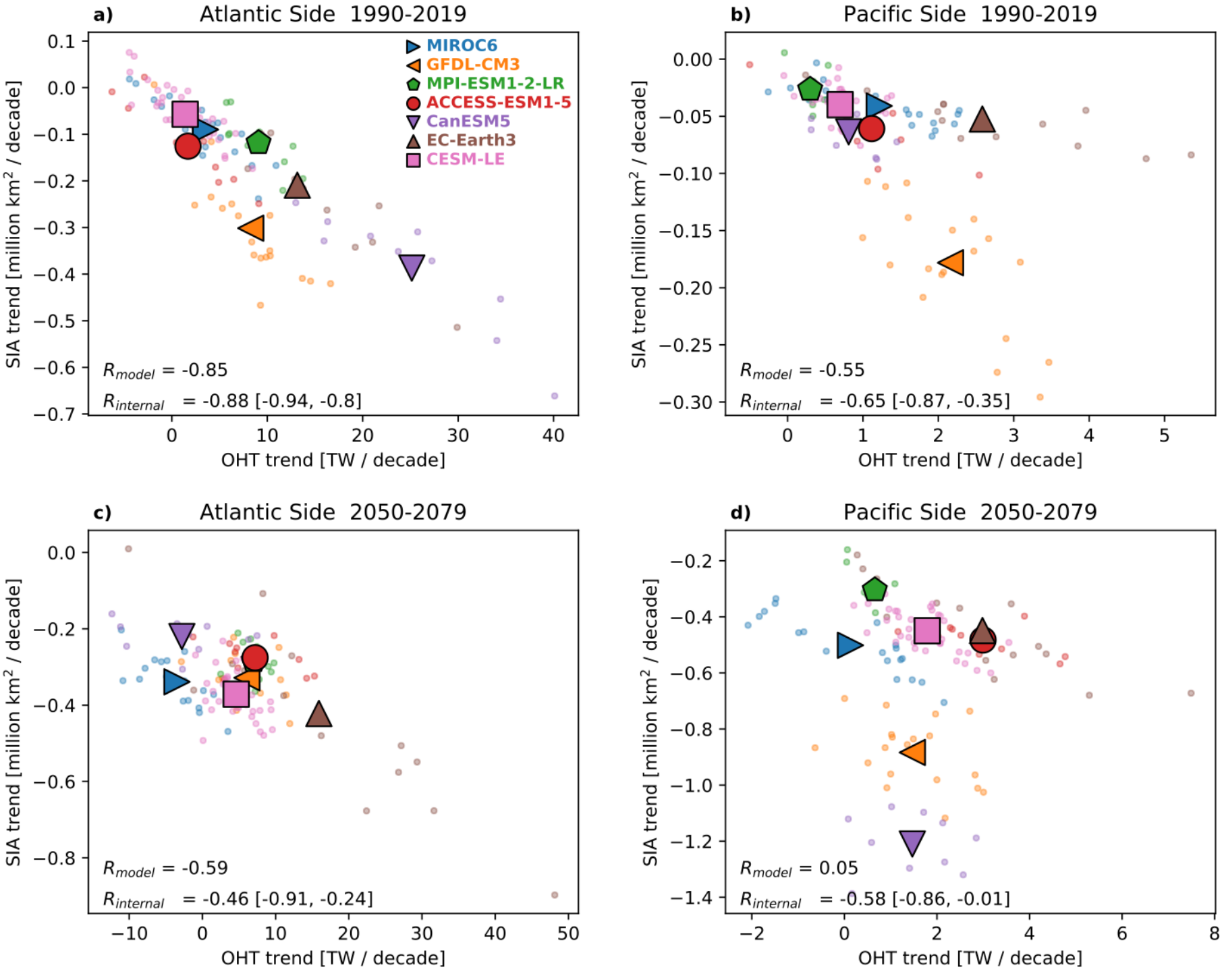
a)
Atlantic Side 1990-2019
MIROC6
GFDL-CM3
MPI-ESM1-2-LR
ACCESS-ESM1-5
CanESM5
EC-Earth3
CESM-LE
SIA trend [million km^2 / decade]
OHT trend [TW / decade]
R_{model} = -0.85
$R_{internal}$ = -0.88 [-0.94, -0.8]
b)
Pacific Side 1990-2019
SIA trend [million km^2 / decade]
OHT trend [TW / decade]
R_{model} = -0.55
$R_{internal}$ = -0.65 [-0.87, -0.35]
c)
Atlantic Side 2050-2079
SIA trend [million km^2 / decade]
OHT trend [TW / decade]
R_{model} = -0.59
$R_{internal}$ = -0.46 [-0.91, -0.24]
d)
Pacific Side 2050-2079
SIA trend [million km^2 / decade]
OHT trend [TW / decade]
R_{model} = 0.05
$R_{internal}$ = -0.58 [-0.86, -0.01]

Figure S1.

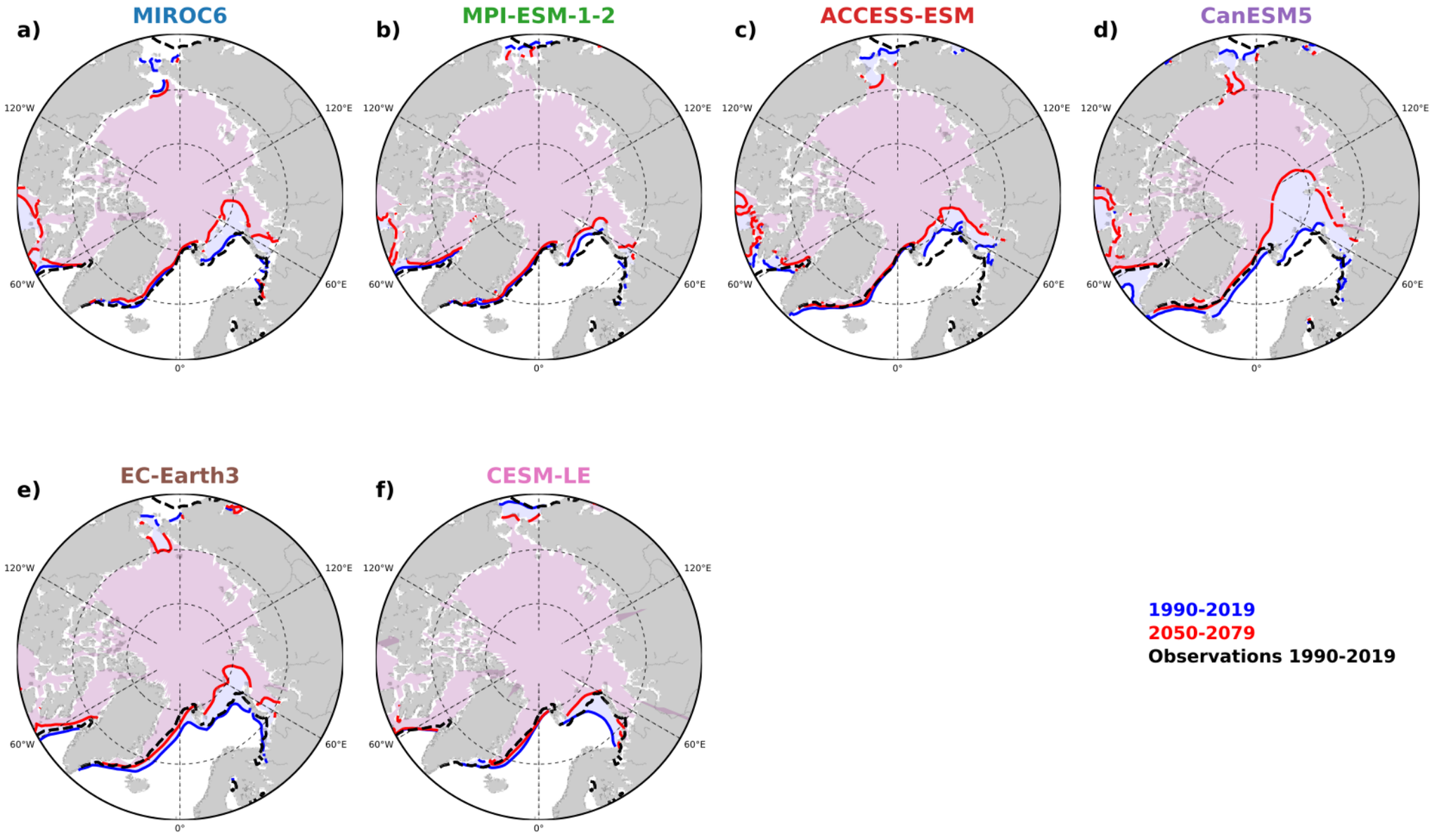
a)
MIROC6
b)
MPI-ESM-1-2
c)
ACCESS-ESM
d)
CanESM5
e)
EC-Earth3
f)
CESM-LE
120°W
120°E
60°W
60°E
0°
1990-2019
2050-2079
Observations 1990-2019

Figure S2.

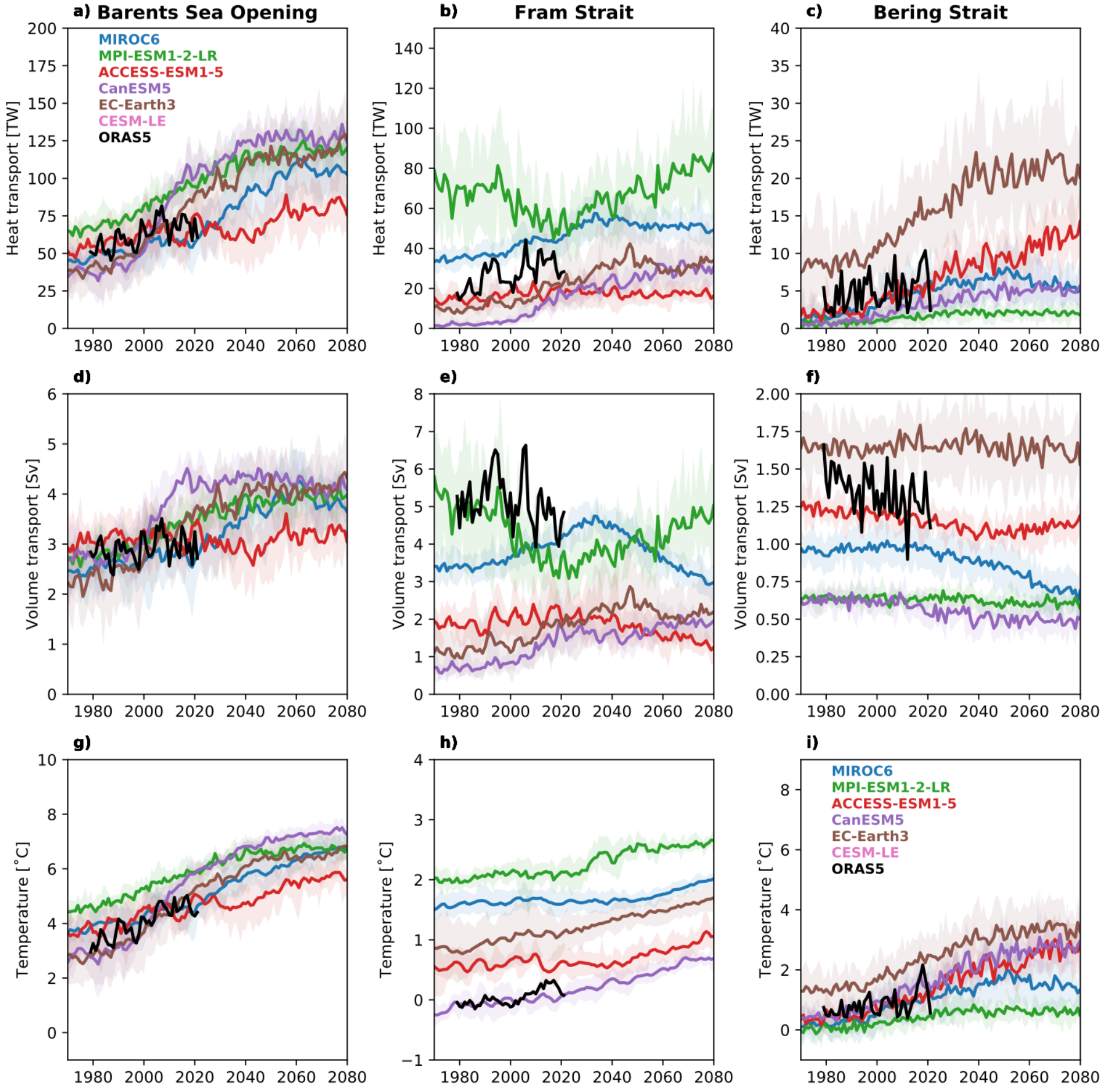
a) Barents Sea Opening
b) Fram Strait
c) Bering Strait
d)
e)
f)
g)
h)
i)
MIROC6
MPI-ESM1-2-LR
ACCESS-ESM1-5
CanESM5
EC-Earth3
CESM-LE
ORAS5
Heat transport [TW]
Volume transport [Sv]
Temperature [˚C]
1980
2000
2020
2040
2060
2080

Figure S3.

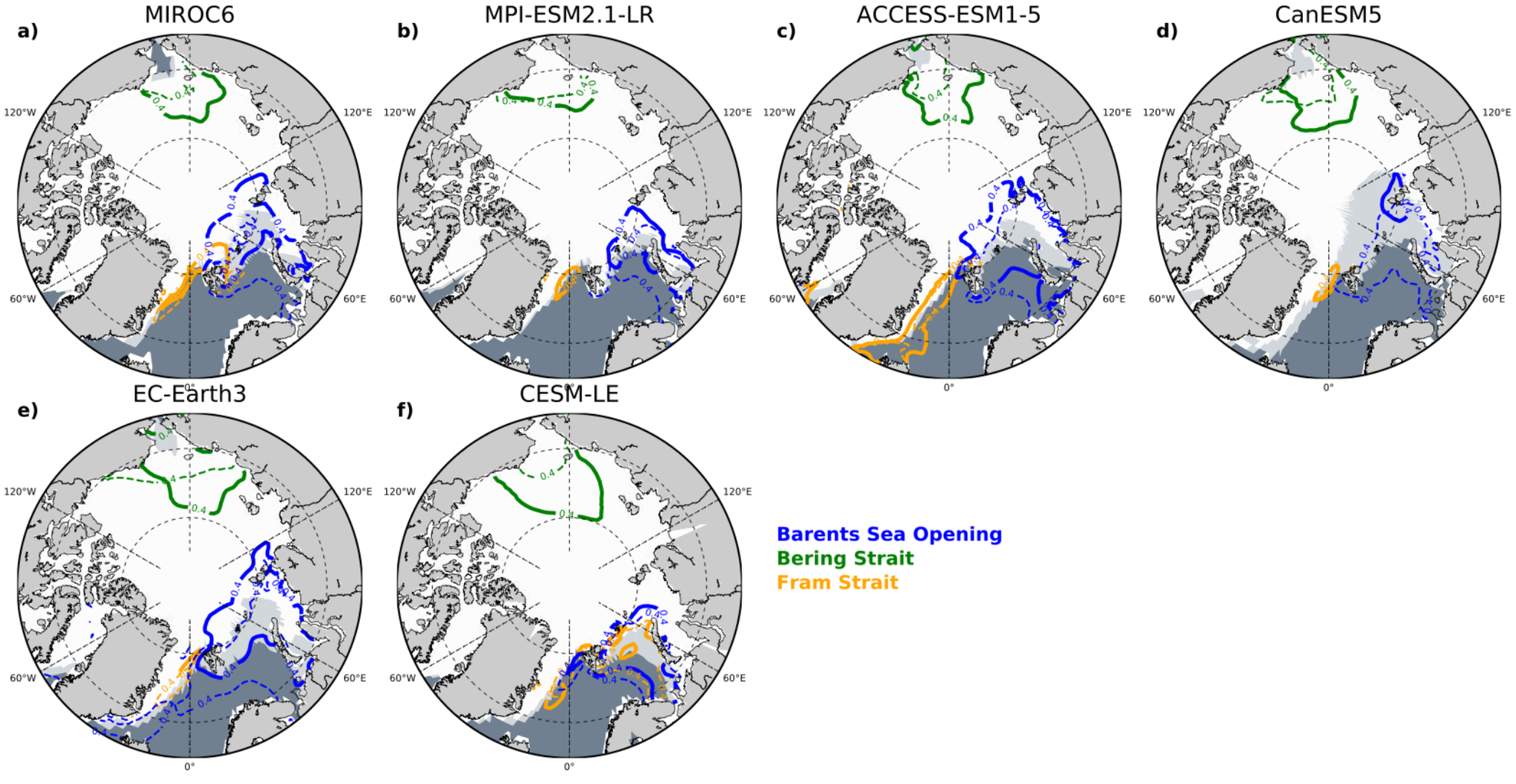
a)
MIROC6
b)
MPI-ESM2.1-LR
c)
ACCESS-ESM1-5
d)
CanESM5
e)
EC-Earth3
f)
CESM-LE
120°W
120°E
60°W
60°E
0°
0.4
Barents Sea Opening
Bering Strait
Fram Strait

Figure S4.

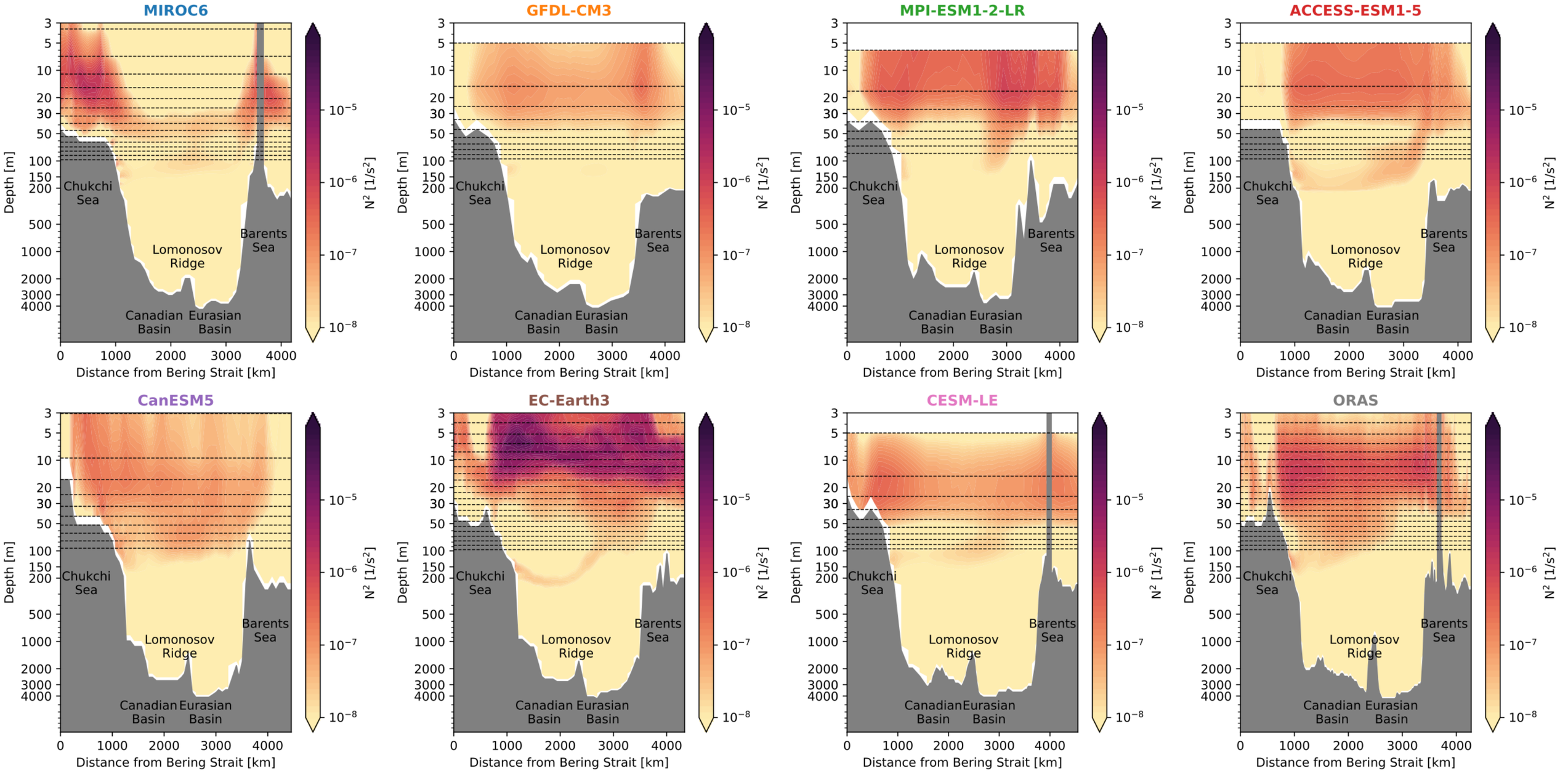
MIROC6
GFDL-CM3
MPI-ESM1-2-LR
ACCESS-ESM1-5
CanESM5
EC-Earth3
CESM-LE
ORAS
Depth [m]
Distance from Bering Strait [km]
N² [1/s²]
Chukchi Sea
Barents Sea
Lomonosov Ridge
Canadian Basin
Eurasian Basin